Review

Ionic Liquids for the Synthesis and Stabilization of Metal Nanoparticles

Christoph Janiak

Institut für Anorganische Chemie und Strukturchemie, Heinrich-Heine-Universität Düsseldorf, Universitätsstrasse 1, D-40225 Düsseldorf, Germany

Reprint requests to Prof. Dr. Christoph Janiak. Fax: +49-(0)211-81-12286.
E-mail: janiak@uni-duesseldorf.de

Z. Naturforsch. **2013**, *68b*, 1059 – 1089 / DOI: 10.5560/ZNB.2013-3140
Received May 31, 2013

Dedicated to Professor Bernt Krebs on the occasion of his 75th birthday

The synthesis and stabilization of metal nanoparticles (M-NPs) from metals, metal salts, metal complexes and metal carbonyls in ionic liquids (ILs) is reviewed. The electrostatic and steric properties of ionic liquids allow for the stabilization of M-NPs without the need of additional stabilizers, surfactants or capping ligands. The synthesis of M-NPs in ILs can be carried out by chemical or electroreduction, thermolysis and photochemical methods including decomposition by microwave or sono-/ultrasound irradiation. Gas-phase syntheses can use sputtering, plasma/glow-discharge electrolysis and physical vapor deposition or electron beam and γ-irradiation. Metal carbonyl precursors $M_x(CO)_y$ contain the metal atoms already in the zero-valent oxidation state needed for M-NPs so that no extra reducing agent is necessary. Microwave-induced thermal decomposition of precursors in ILs is a rapid and energy-saving access to M-NPs because of the significant absorption efficiency of ILs for microwave energy due to their ionic charge, high polarity and high dielectric constant. M-NP/IL dispersions can be applied in catalytic reactions, *e. g.*, in C–C coupling or hydrogenation catalysis.

Key words: Metal Nanoparticles, Ionic Liquids, Metal Carbonyls, Microwave Irradiation, Catalysis

Introduction

Metal nanoparticles (M-NPs) are of increasing interest in various technologies [1]. In a "bottom-up" approach, M-NPs can be prepared as dispersions by reduction of metal salts or by photolytic, sonolytic or thermal decomposition of metal-organic precursors in various solvents [2]. The controlled and reproducible synthesis of defined and stable M-NPs with a small size distribution is very important for a range of applications [3 – 7]. The synthesis of metal nanoparticles with defined sizes and morphologies can be tailored through the synthesis conditions such as temperature, solvent, pressure and the choice of stabilizing agent [8]. In the literature nanoparticles are also referred to as nanophase clusters, nanocrystals and colloids. Here we will mainly use the generic term nanoparticles for simplicity. The chemistry and physics of nanoparticles with their high surface-to-volume ratio is dominated by their surface energy [9]. The smaller the nanoparticle is, the larger is the fraction of exposed surface atoms. The latter determine the physics and chemistry of nanoparticles with their "unsaturated bonds". M-NPs are investigated as "soluble" analogs of heterogeneous catalysts [10 – 16]. The activity of (heterogeneous) catalysts benefits strongly from a high surface area. Yet, small NPs are only kinetically stable and will aggregate to thermodynamically more stable larger particles (Fig. 1).

This agglomeration is based on the principles of the Ostwald ripening [17, 18] as a thermodynamically driven spontaneous process because larger particles are more energetically favored than smaller ones. This fact originates from coordinatively unsaturated surface atoms which are energetically less stable than well-ordered and fully coordinated atoms in the bulk. Large particles, with their lower surface to volume ratio, present a lower energy state with a lower surface energy. The system lowers its overall energy by releasing atoms from the surface of a small (energetically unfavorable) particle which diffuse through solution and then attach to the surface of a larger particle. Conse-

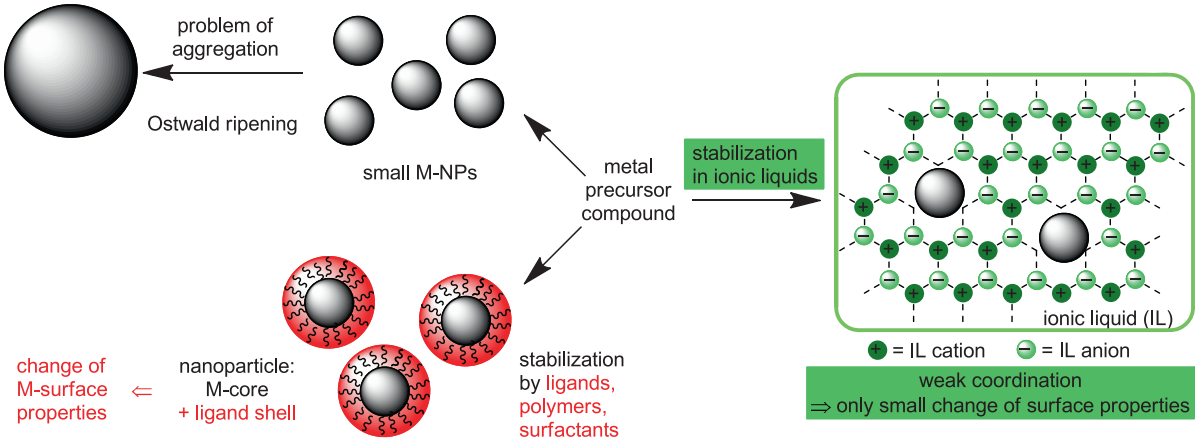

Fig. 1 (color online). Schematic presentation of the stabilization of metal nanoparticles (M-NP) through protective stabilizers or in ionic liquids to prevent aggregation.

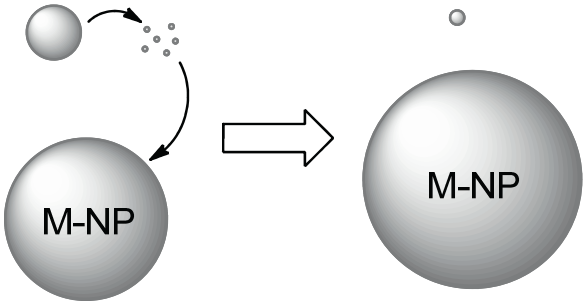

Fig. 2. Schematic presentation of the Ostwald ripening of metal nanoparticles (M-NPs).

quently, the number of smaller particles diminishes at the expense of the growth of larger particles (Fig. 2).

Therefore, small metal nanoparticles require stabilization through additives which build up a protective layer to shield the particles from each other. Bilayers of surfactant ions lead to an electrostatic stabilization. Surface-capping ligands or polymers give a protective layer which provides steric coverage to prevent agglomeration (*cf.* Fig. 1) [19 – 22]. For catalytic application this surface coverage also means at least partial desactivation. In ionic liquids (ILs) metal nanoparticles can be synthesized and stored for some time without any additional stabilizers. The electrostatic and steric ("electrosteric") properties of ionic liquids can stabilize M-NPs without the need of surfactants, polymers or capping ligands (*cf.* Fig. 1). ILs may be regarded as a "nanosynthetic template" [23] that stabilizes M-NPs on the basis of their ionic nature [24], high polarity, high dielectric constant and supramolecular network, without the need of additional protective ligands (*cf.* Fig. 4) [25 – 30].

Ionic Liquids (ILs)

Ionic liquids are liquid (molten) salts of weakly coordinating cations and anions (Fig. 3). By definition the melting point of ILs has to be below 100 °C. ILs that are liquid at room temperature are termed RT-ILs [31 – 34]. The liquid state is favored by small lattice enthalpies and large entropy changes, due to the large size and conformational flexibility of the weakly coordinating ions [35]. ILs have decisively different physical properties than other organic solvents, including high charge density, high polarity, high dielectric constant and supramolecular network formation [28]. Typical IL cations are 1-alkyl-3-methyl-imidazolium and tetraalkylammonium, and typical anions for ILs are halide anions, tetrafluoroborate BF_4^-, hexafluorophosphate PF_6^-, trifluoromethanesulfonate (triflate) TfO^-, $CF_3SO_3^-$, and bis(trifluoromethylsulfonyl)amide Tf_2N^-, $(CF_3SO_2)_2N^-$ (Fig. 3) [12, 36].

Ionic liquids are unique alternatives to traditional aqueous or organic solvents [37]. Over the last years they have been introduced into solution chemistry and intensively investigated as a new liquid medium [38, 39]. The preparation of advanced functional ma-

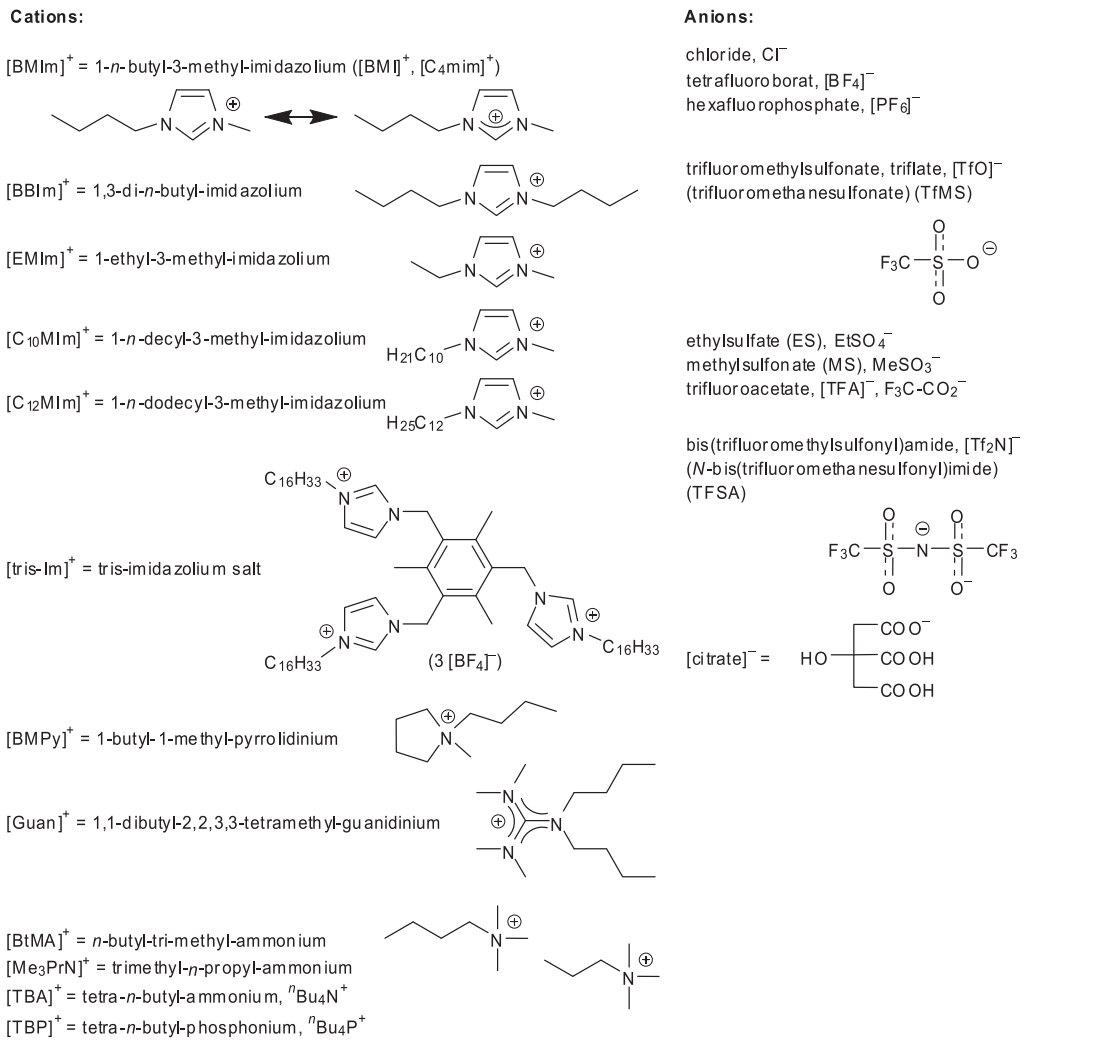

Fig. 3. Cations and anions of non-functionalized ILs. Abbreviations and the use of capital or small letters, charges added and brackets around abbreviations vary in the literature. For functionalized ILs, see Fig. 5.

terials making use of ILs, through ionothermal synthesis, has been shown to be very promising [40 – 42]. The use of ILs and the concomitant ionothermal method is increasing because of the excellent solvent properties of ILs, such as negligible vapor pressure, high thermal stability, high ionic conductivity, a broad liquid-state temperature range, and the ability to dissolve a variety of materials [43, 44].

Properties of ILs can be designed through the combination of cations and anions. For example, ILs containing Tf_2N^- offer low viscosity and high electrochemical and thermal stability [45]. If bis(trifluoromethylsulfonyl)amide Tf_2N^- is replaced by bis(methylsulfonyl)amide, viscosity increases and stability decreases [46]. Neutron scattering experiments on crystalline, glassy, and liquid samples of imidazolium ILs have suggested that ILs have an organizational behavior intermediate between isotropic liquids and liquid crystals [31]. ILs have an intrinsic "nanostructure" which is caused by electrostatic, hydrogen bonding and van-der-Waals interactions [26, 31]. The mesoscopic structure of especially imidazolium ionic liquids can be described in part as a supramolecular three-dimensional hydrogen-bonded

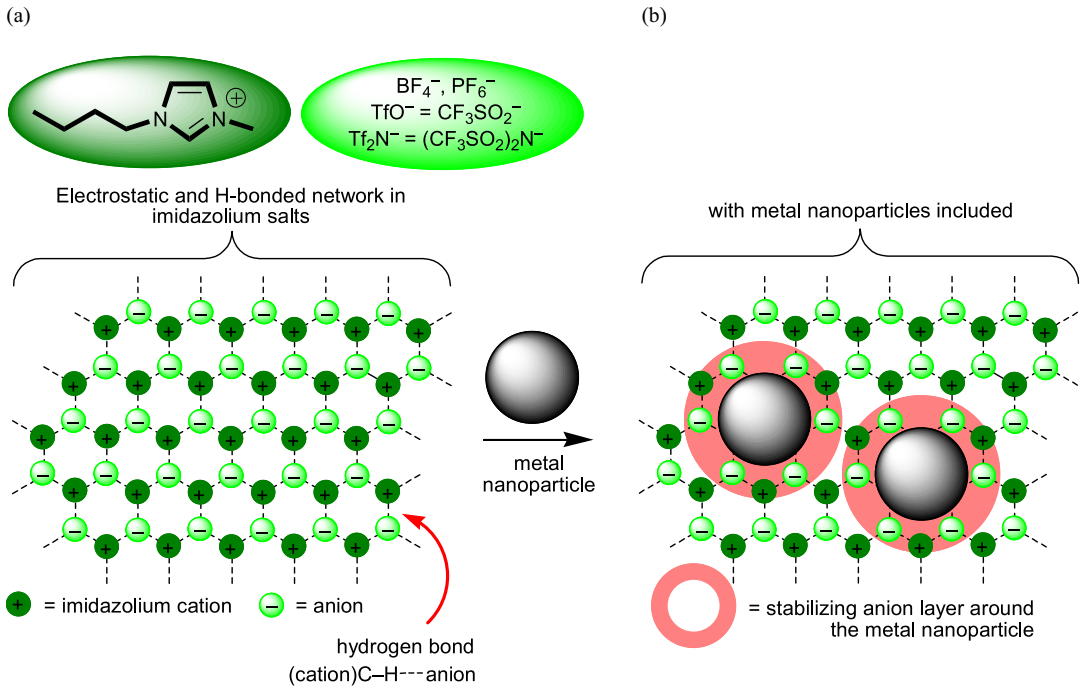

Fig. 4 (color online). (a) Schematic network structure in 1,3-dialkyl-imidazolium-based ionic liquids projected in two dimensions. (b) The inclusion of metal nanoparticles (M-NPs) in the supramolecular IL network with electrostatic and steric (= *electrosteric*) stabilization is indicated through the formation of the suggested primary anion layer forming around the M-NPs. (Adapted from ref. [30] with permission from the author; © 2011 Elsevier B. V.).

network [26, 28, 29]. This structural pattern is not only seen in the solid phase, but is also maintained to a great extent in the liquid phase. The introduction of other molecules and macromolecules proceeds with a disruption of the hydrogen bonding network and in some cases can generate nano-structures with polar and nonpolar regions where inclusion-type compounds can be formed [25, 26]. When mixed with other molecules or M-NPs, ILs become nanostructured materials with polar and nonpolar regions [47 – 50]. The combination of undirected Coulomb forces and directed hydrogen bonds leads to a high attraction of the IL building units. This is the origin of their (high) viscosity, negligible vapor pressure and three-dimensional constitution. The IL network properties should be well suited for the synthesis of defined metal nanoparticles (see Fig. 4) [25 – 27].

Metal Nanoparticles and Ionic Liquids

Some reviews note a parallel and synergistic development of both nanoparticles and ionic liquids for materials chemistry [27], while others devote only a short section to the use of ionic liquids in the synthesis of inorganic nanoparticles [51].

The inclusion of metal nanoparticles in the supramolecular ionic liquid network supplies the necessary electrostatic and steric (= *electrosteric*) stabilization through the formation of an ion layer around the M-NPs. The type of this ion layer, and hence the mode of stabilization of metal nanoparticles in ILs, is still a matter of some discussion [27, 52]. Aside from the special case of thiol-, ether-, carboxylic acid-, amino-, hydroxyl- and other functionalized ILs (see Fig. 5 and accompanying text) one could assume IL-cation or -anion coordination to the NP surface. The electrostatic stabilization of a negatively charged surface of Au-NPs by parallel coordination mode of the imidazolium cation was proposed on the basis of surface-enhanced Raman spectroscopy (SERS) studies (*cf.* Fig. 6a) [53]. This proposal was supported by the finding of a negative zeta potential of M-NPs prepared by chemical reduction processes in aqueous solutions [54].

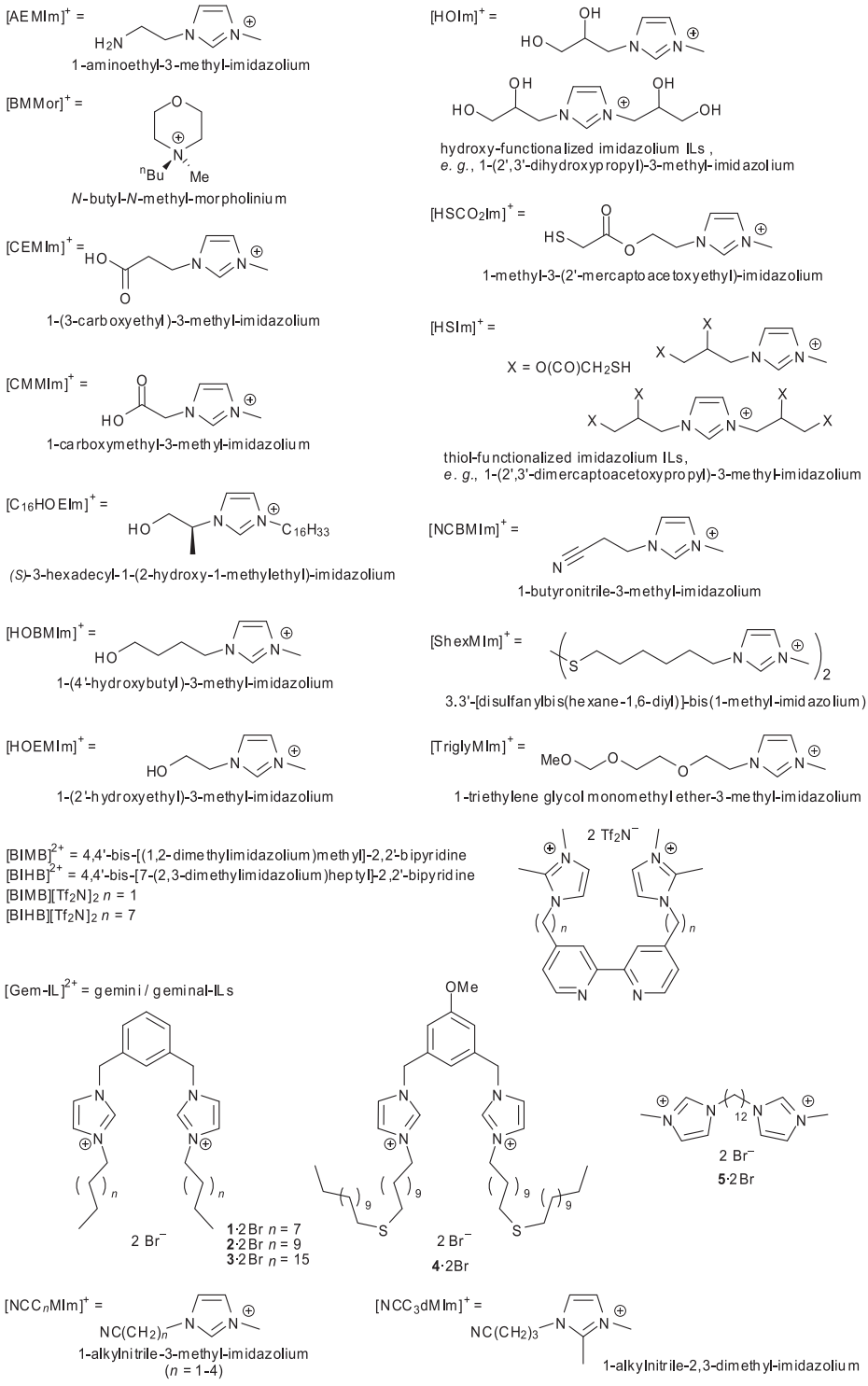

Fig. 5. Examples of functionalized imidazolium-ILs [52, 53, 67 – 70].

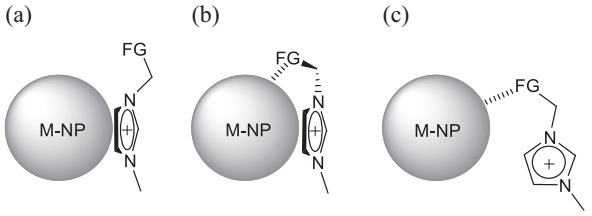

Fig. 6. Possible stabilization modes of metal nanoparticles by IL-imidazolium cations with functional groups (FG) [78].

According to DLVO (Derjaugin-Landau-Verwey-Overbeek) theory [55], ILs provide an electrostatic protection in the form of a "protective shell" for M-NPs [56 – 61]. DLVO theory predicts that the first inner shell must be anionic and the anion charges should be the primary source of stabilization for the electrophilic metal nanocluster [55]. DLVO theory treats anions as ideal point charges. Real-life anions with a molecular volume would be better classified as "electrosteric stabilizers" meaning to combine both the electrostatic and the steric stabilization. However, the term "electrosteric" is contentious and ill-defined [62]. The stabilization of metal nanoclusters in ILs could, thus, be attributed to "extra-DLVO" forces [62] which include effects from the network properties of ILs such as hydrogen bonding, hydrophobicity and steric interactions [4, 63].

Density functional theory (DFT) calculations in a gas-phase model favor interactions between IL anions, such as BF_4^-, instead of imidazolium cations and Au_n clusters ($n = 1, 2, 3, 6, 19, 20$). This suggests Au···F interactions and anionic Au_n stabilization in fluorous ILs. A small and Au concentration-dependent ^{19}F NMR chemical shift difference (not seen in ^{11}B or ^{1}H NMR) for Au-NP/[BMIm][BF_4] supports the notion of a BF_4^- fluorine···Au-NP contact seen as crucial for the NP stabilization in dynamic ILs [64]. DFT calculations also indicate a weak covalent part in this Au···F interaction. Free imidazole bases (*e. g.* 1-methyl-imidazole) show similar binding energies. The Cl^- anions have the highest binding energy and can therefore be expected to bind to the NP if present in the solution. At the same time no significant binding of the $[BMIm]^+$ or MIm^+ imidazolium cations was found. These findings support the model of preferred interaction between anions and Au-NPs, but also confirm the importance to consider a possible presence of Cl^- anions in the ionic liquid solution [64, 65].

A combined DFT/vibrational spectroscopy approach found that palladium nanoparticles interact more strongly with the BF_4^- anions than with the 1,3-dimethyl-imidazolium ($[MMIm]^+$) and 1-ethyl-3-methyl-imidazolium ($[EMIm]^+$) cations of the used ILs. This suggested an important role of the anions in Pd-NP formation and stabilization in ILs. At the same time, the binding between isolated Pd atoms and the C atoms of the 1,3-dimethyl-imidazolium cation is stronger than Pd–[BF_4^-] binding [66].

Functionalized imidazolium-ILs stabilize aqueous dispersions of metal NPs much more efficiently than non-functionalized imidazolium-ILs (*cf.* Fig. 3), because of the added functional group. Thiol- [67 – 69], ether- [53], carboxylic acid- [52], amino- [52, 70], and hydroxyl- [68, 71, 72] or nitrile- [73 – 75] imidazolium-ILs (Fig. 5) have been used to synthesize and stabilize noble metal, primarily gold, NPs. The functional groups on the imidazolium cations exert an additional stabilization on M-NPs because of ligand-donor interactions of the functional group with the particle surface. The donor atom(s) of the functional group can attach to the metal nanoparticle much like an extra stabilizing capping ligand [52]. Then, the stabilization of metal nanoparticles in functionalized imidazolium-based ILs occurs through the cation with its functional group (Fig. 6) [76, 77]. For both non-functionalized and functionalized ILs equally charged layers around the M-NPs lead to their separation through electrostatic repulsion and, thus, prevent their aggregation or Ostwald ripening [17, 78].

Synthesis of Metal Nanoparticles in Ionic Liquids

Metal nanoparticles can be synthesized in ionic liquids [79] through chemical reduction [80 – 85] or decomposition [86 – 89], by means of photochemical reduction [90, 91] or electro-reduction/electrodeposition [92 – 94] of metal salts where the metal atom is in a formally positive oxidation state. An elegant route is also the thermal, photolytic or chemical decomposition of compounds with zero-valent metal atoms, such as metal carbonyls $M_x(CO)_y$ [23, 85, 95, 96] or [Ru(COD)(COT)] (see section *Metal nanoparticles from zero-valent metal precursors*) [97, 98]. Common to the synthesis of M-NPs in ILs is that no extra stabilizing molecules or organic solvents are needed [19, 25, 27, 61, 99], even if in some cases such stabilizers are added.

Even without a chemical reaction (as exemplified below) simple dis-agglomeration of micro-sized copper flakes (1 – 5 μm) by stirring in ILs for 24 h at room temperature yielded copper nanoparticles of 50 – 100 nm diameter in [BMIm][BF_4] and of 80 – 100 nm diameter in [BMIm][PF_6] and [EMIm][BF_4]. A positive charge density of the Cu-NPs was deduced by XPS, owing to the strong interactions between the surface of copper nanoparticles and the anion of [BMIm][BF_4] [100].

Chemical reduction

The reduction of metal salts is the most utilized method to generate M-NPs in ILs in general. A myriad of M-NPs have been prepared in ILs from compounds with the metal in a formally positive oxidation state M^{n+}, including M = Rh [82], Ir [101], Pt [102], Ag [80, 103], Au [67], as listed in Table 1. Many different types of reducing agents are used, like gases (H_2), organic (citrate, ascorbic acid, imidazolium cation of IL) and inorganic ($NaBH_4$, $SnCl_2$) agents (Table 1).

Molecular hydrogen (H_2) or sodium borohydride ($NaBH_4$) are often used as the reductants. The synthesis of M-NPs by reduction is not limited to conventional batch scale glass flasks. Microfluidic reactors with various continuous-flow configurations have been reported for the fabrication of metal nanoparticles including cobalt, copper, platinum and palladium, gold and silver, and core-shell particles [133].

Table 1. Examples of M-NPs prepared in ILs by chemical reduction.

Metal	Metal salt precursor	Reducing agent	Ionic liquid[a]	M-NP average diameter ± standard deviation (nm)	Ref.
Monometallic					
Rh	$RhCl_3 \cdot 3H_2O$	H_2, 75 °C and 4 bar	[BMIm][PF_6]	2.0–2.5	[82]
	[Rh(COD)-μ-Cl]$_2$[b]	H_2 + laser radiation	[BMIm][PF_6]	7.2 ± 1.3	[104]
	$RhCl_3$	$NaBH_4$	[BMIm][Tf_2N] / [BIMB][Tf_2N]$_2$ or [BIHB][Tf_2N]$_2$	1 – 3	[105]
Ir	[Ir(COD)Cl]$_2$[b]	H_2, 75 °C and 4 bar	[BMIm][BF_4], [BMIm][PF_6], [BMIm][TfO]	2 – 3	[106]
	[Ir(COD)$_2$]BF_4, [Ir(COD)Cl]$_2$[b]	H_2	[1-alkyl-3-methyl-Im][BF_4]	irregular 1.9 ± 0.4, 3.6 ± 0.9	[84]
Pd	H_2PdCl_4	$NaBH_4$	[$HSCO_2$Im][Cl]	nanowires	[69]
	H_2PdCl_4	$NaBH_4$	[Guan][Br] / Vulcan-72 carbon	~2.8	[107]
	$PdCl_2$	H_2 + laser radiation	[BMIm][PF_6]	4.2 ± 0.8	[104]
	Pd(acac)$_2$	H_2	[BMIm][PF_6]	10 ± 0.2	[87]
	Pd(acac)$_2$	imidazolium ILs, thermal, see text	[BMIm][PF_6], [HOBMIm][Tf_2N]	5, 10, catal. for select. acetylene hydrogenation	[87]
	Pd(OAc)$_2$ or $PdCl_2$	imidazolium ILs, ultrasound, see text	[BBIm][Br], [BBIm][BF_4]	20, catalyst for Heck reactions	[88, 134]
	Pd(OAc)$_2$	[BMIm][Tf_2N], thermal	[BMIm][Tf_2N] / PPh_3	~1, catalyst for Heck reactions	[89, 134]
	Pd(OAc)$_2$	imidazolium ILs, thermal, see text	[HOEMIm][TfO] [HOEMIm][TFA] [HOEMIm][BF_4] [HOEMIm][PF_6] [HOEMIm][Tf_2N] [BMIm][Tf_2N]	2.4 ± 0.5 2.3 ± 0.4 3.3 ± 0.6 3.1 ± 0.7 4.0 ± 0.6 6.2 ± 1.1	[72]
	Pd(OAc)$_2$		[TBA][Br] / [TBA][OAc]	3.3 ± 1.2, catalyst for Heck arylations	[109, 110, 134]

Table 1. Continued.

Metal	Metal salt precursor	Reducing agent	Ionic liquid[a]	M-NP average diameter ± standard deviation (nm)	Ref.
	$Pd(OAc)_2$		[BtMA][Tf_2N]	catalyst for Heck cross-coupling	[111, 134]
	$Pd(OAc)_2$	imidazolium IL, thermal, see text	[NCBMIm][Tf_2N]	7.3 ± 2.2	[112]
	$Pd_2(dba)_3$	H_2, 3 atm	[tris-Im][BF_4]$_3$, see Fig. 3	catalyst for Suzuki cross-coupling	[113, 134]
	bis(benzothiazolylidene carbene)PdI_2		[TBA][Br] / [TBA][OAc]	catalyst for Heck arylations	[109]
Pt	$Na_2Pt(OH)_6$	$NaBH_4$	[HSIm][A] or [HOIm][A], A = Cl^- or HS-$(CH_2)_3$-SO_3^-	3.2 ± 1.1 2.2 ± 0.2 2.0 ± 0.1	[68]
	H_2PtCl_6	$NaBH_4$	[CMMIm][Cl], [AEMIm][Br]	2.5	[52]
	$H_2Pt(OH)_6$	HCOOH	[BMIm][FEP] [FEP] = [$PF_3(C_2F_5)_3$]$^-$	no or different co-stabilizers, 1.7 – 3.4 nm, also immobilized on supports, cat. for nitrostyrene hydrogenation	[114]
	$H_2Pt(OH)_6$	HCOOH	H_2O/[BMIm][PF_6], H_2O/[BMIm][FEP], also with cinchonidine chiral costabilizer	2.9 ± 0.7 3.1 ± 0.7 $1.8 – 2.3 \pm 0.8$, catalysts for enantioselect. hydrogenation	[115]
	PtO_2	H_2	[BMIm][BF_4], [BMIm][PF_6]	2 – 3	[116]
	$Pt_2(dba)_3$[c]	H_2, 75 °C, 4 atm	[BMIm][PF_6]	2.0 – 2.5	[102]
	(MeCp)$PtMe_3$	imidazolium ILs, MWI, hv, thermal, see text	[BMIm][BF_4], [BtMA][Tf_2N]	1.5 ± 0.5, see text	[117]
Cu	$Cu(OAc)_2 \cdot H_2O$	$H_2NNH_2 \cdot H_2O$ (hydrazine hydrate)	[BMIm][BF_4] [BMIm][PF_6] each w. 1 % PVP or PVA as stabilizer[d]	spherical, PVP: 80 – 130, PVA: 260 cubic, PVP: 160 ± 14; catalyst in click reaction	[118]
Ag	$AgBF_4$	H_2, 85 °C, 4 atm BIm as scavenger, see text	[BMIm][BF_4] [BMIm][PF_6] [BMIm][TfO] [BtMA][Tf_2N]	2.8 ± 0.8 4.4 ± 1.3 8.7 ± 3.4 26.1 ± 6.4	[97]
	$AgBF_4$	H_2	[BMIm][BF_4] [BMpy][TfO] with TX-100/cyclohexane as reverse micellar system	~9 (DLS), ~11 (DLS), both ~3 from TEM	[119]
	$AgBF_4$	[BMIm][BH_4], 1-MeIm as scavenger	[BMIm][Tf_2N] in microfluidic reactor	3.73 ± 0.77	[133]
	$AgBF_4$	[BMIm][BH_4]	[BMIm][BF_4] purified and H_2O, Cl^- or MIm impurity-spiked	4.4 ± 0.8 $4.0 – 4.5 \pm 0.9$ $3.8 – 3.9 \pm 0.7$ $3.8 – 4.4 \pm$ ~0.7	[120]

Table 1. Continued.

Metal	Metal salt precursor	Reducing agent	Ionic liquid[a]	M-NP average diameter ± standard deviation (nm)	Ref.
	Ag_2CO_3	Me_2NCHO (DMF)	$[Me_2NH_2][Me_2NCO_2]$ with small amounts of DMF	2 – 14	[103]
	$AgNO_3$	Tween 85	[BMIm][PF_6]	3 – 10	[121]
Au	$HAuCl_4$	Na_3citrate/ $NaBH_4$, Na_3 citrate, ascorbic acid	[EMIm][$EtSO_4$]	9.4, 3.9, nanorods	[143]
	$HAuCl_4$	ascorbic acid	[BMIm] [$C_{12}H_{25}OSO_3$] (lauryl sulfate)	20 – 50	[122]
	$HAuCl_4$	Na_3citrate	[CMMIm][Cl], [AEMIm][Br]	23 – 98	[52]
	$HAuCl_4 \cdot 3H_2O$	$H_2NNH_2 \cdot H_2O$ (hydrazine monohydrate)	[TriglyMIm][$MeSO_3$]	~7.5	[53]
	$HAuCl_4$	$NaBH_4$	[ShexMIm][Cl]	5.0	[67]
	$HAuCl_4$	$NaBH_4$	[HSIm][A] or [HOIm][A], A = Cl^- or HS-$(CH_2)_3$-SO_3^-	3.5 ± 0.7, 3.1 ± 0.5, 2.0 ± 0.1	[68]
	$HAuCl_4$	$NaBH_4$	[CMMIm][Cl], [AEMIm][Br]	3.5	[52]
	$[C_{16}HOEIm]AuCl_4$ from $[C_{16}HOEIm]Br$ and $HAuCl_4$	$NaBH_4$	$CHCl_3/H_2O$, $[C_{16}HOEIm][Br]$	6.0 ± 1.4	[123]
	$HAuCl_4$	$NaBH_4$	[Gem-IL][$Br]_2$ **1** · 2Br–**4** · 2Br, see Fig. 5	**3**: 8.8 ± 2.2 **4**: 5.3 ± 2.4	[124]
	$HAuCl_4$	$NaBH_4$	[BMIm][BF_4] in microfluidic reactor	4.38 ± 0.53	[125]
	$HAuCl_4$	$NaBH_4$	[BMIm][PF_6]	4.8 ± 0.7 (5.3 ± 0.8 after 2 weeks)	[126]
	$HAuCl_4$	$NaBH_4$	[BMIm][PF_6] / [AEMIm][PF_6]	4.3 ± 0.8	[126]
	$HAuCl_4$	$NaBH_4$	[C_{12}MIm][Br]	8.2 ± 3.5, stable for at least 8 months	[127]
	$HAuCl_4$	$NaBH_4$	[Gem-IL][$Br]_2$ **5** · 2Br, see Fig. 5	10.1 ± 4.2	[127]
	$HAuCl_4$	[BMIm][BH_4], 1-MeIm as scavenger	[BMIm][Tf_2N] in microfluidic reactor	4.28 ± 0.84	[133]
	$HAuCl_4 \cdot 3H_2O$	$NaBH_4$, cellulose	[BMIm][Cl]	9.7 ± 2.7	[128]
	$HAuCl_4$	cellulose, see text	[BMIm][Cl]	300 – 800	[83]
	$HAuCl_4 \cdot 3H_2O$	glycerol	[EMIm][TfO], [EMIm][$MeSO_3$], [EMIm][$EtSO_4$]	5 – 7, low temp. 5 – 7, aggregate at higher temp. 15 – 20, polydisperse	[129]
	$HAuBr_4$	Me_2NCHO (DMF)	$[Me_2NH_2][Me_2NCO_2]$ with small amounts of DMF	2 – 4	[103]
	Au(CO)Cl	imidazolium ILs, thermal, MWI, hv, see text	[BMIm][BF_4]	1.8 ± 0.4, 4.1 ± 0.7	[64]

Table 1. Continued.

Metal	Metal salt precursor	Reducing agent	Ionic liquid[a]	M-NP average diameter ± standard deviation (nm)	Ref.
	$KAuCl_4$	[BMIm][BF_4] thermal, see text	[BMIm][BF_4]	1.1 ± 0.2	[64]
	$HAuCl_4 \cdot 4H_2O$	[$Me_3NC_2H_4OH$] [Zn_nCl_{2n+1}], thermal	[$Me_3NC_2H_4OH$] [Zn_nCl_{2n+1}]	135 °C: 35 ± 12, 140 °C: 30 ± 4, 145 °C: 24 ± 3	[130]
	$HAuCl_4 \cdot 3H_2O$,	[BMIm][BF_4], ultrasound, see text.	[BMIm][BF_4] / MWCNT[e]	10.3 ± 1.5	[153]
	$KAuCl_4$	$SnCl_2$	[BMIm][BF_4]	2.6 – 200	[65]
	$AuCl_3 \cdot 3H_2O$	[TBP][citrate]	[TBP][citrate]	15 – 20	[131]
	$Au(OAc)_3$	imidazolium IL, thermal	[HOEMIm][Tf_2N]	4.3 ± 0.9	[108]
Bimetallic					
Au-Pd 1 : 3	K_2PdCl_4, $HAuCl_4$	$NaBH_4$	[BMIm][PF_6]	5.3 ± 3.0	[126]
			[BMIm][PF_6] / [AEMIm][PF_6]	3.6 ± 0.7	[126]
$Au_{0.8}Pd_{0.2}$	$Pd(OAc)_2$, $Au(OAc)_3$	imidazolium IL, thermal	[HOEMIm][Tf_2N]	4.0 ± 0.5	[108]
$Au_{0.5}Pd_{0.5}$				4.4 ± 0.5	
$Au_{0.2}Pd_{0.8}$				4.0 ± 0.8	
$AuPd_4$, $AuPd_4$/CNT	$(NH_4)_2PdCl_6$, $HAuCl_4 \cdot 4H_2O$	Triton X-100 alcohol reductant	H_2O/Triton X-100/ [BMIm][PF_6] (CNT)	4.5	[132]

[a] For non-functionalized ILs, see Fig. 3, for functionalized ILs, see Fig. 5; [b] COD = 1,5-cyclooctadiene, COT = 1,3,5-cyclooctatriene; [c] dba = bis-dibenzylidene acetone; [d] PVP = polyvinyl pyrrolidone, PVA = polyvinyl alcohol; [e] MWCNT = multi-walled carbon nanotube.

Pd-NPs from palladium(II) salts could be synthesized in the presence of imidazolium-based ILs without the need for an additional reducing agent. It is suggested that formation of Pd-*N*-heterocyclic carbene complexes as intermediates takes place preceding the formation of Pd-NPs (Fig. 7) [88, 134]. The participation of carbene species in imidazolium ILs was supported by D/H exchange reactions at C2, C4 and C5 of the imidazolium cation in catalytic hydrogenation reactions promoted by classical Ir(I) colloid precursors and Ir-NPs in deuterated imidazolium ILs [135]. Imidazolium salts are also known as precursors for stable carbenes and as mild reducing agents [136].

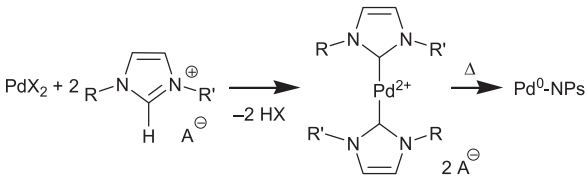

Fig. 7. Reduction of Pd(II) species with an imidazolium-based IL through intermediate formation of Pd carbene complexes. Decomplexation and reduction occurs during heating [134].

Thermal decomposition of $Pd(OAc)_2$ works well in various, also common organic solvents [137 – 139]. Pd-NPs with a diameter of ~ 1 nm were formed from $Pd(OAc)_2$ in [BMIm][Tf_2N] simply by heating to 80 °C in the presence of PPh_3 [89]. Monodisperse Pd nanoparticles of 5 and 10 nm were obtained from $Pd(acac)_2$ dissolved in [HOBMIm][Tf_2N] by heating in the absence of an additional reducing agent [87]. Heating (120 °C) of $Pd(OAc)_2$ in 1-butyronitrile-3-methyl-imidazolium *N*-bis(trifluoromethane sulfonyl)amide [NCBMIm][Tf_2N] under reduced pressure leads to the formation of stable and small-sized Pd-NPs [112].

Pd-NPs were prepared from $Pd(OAc)_2$ in hydroxy-functionalized ILs with the 1-(2′-hydroxyethyl)-3-methyl-imidazolium $[HOEMIm]^+$ cation and non-functionalized control IL by thermal treatment. Based on a determinaton of the percentage of $Pd(OAc)_2$ remaining in the sample, the influence of the anions on the decomposition rate of $Pd(OAc)_2$ was given the order $[Tf_2N]^-$, $[PF_6]^- > [BF_4]^- > [OTf]^- > [TFA]^-$ in a series of hydroxy-functionalized ILs with the $[HOEMIm]^+$ cation. The OH-functionalized IL

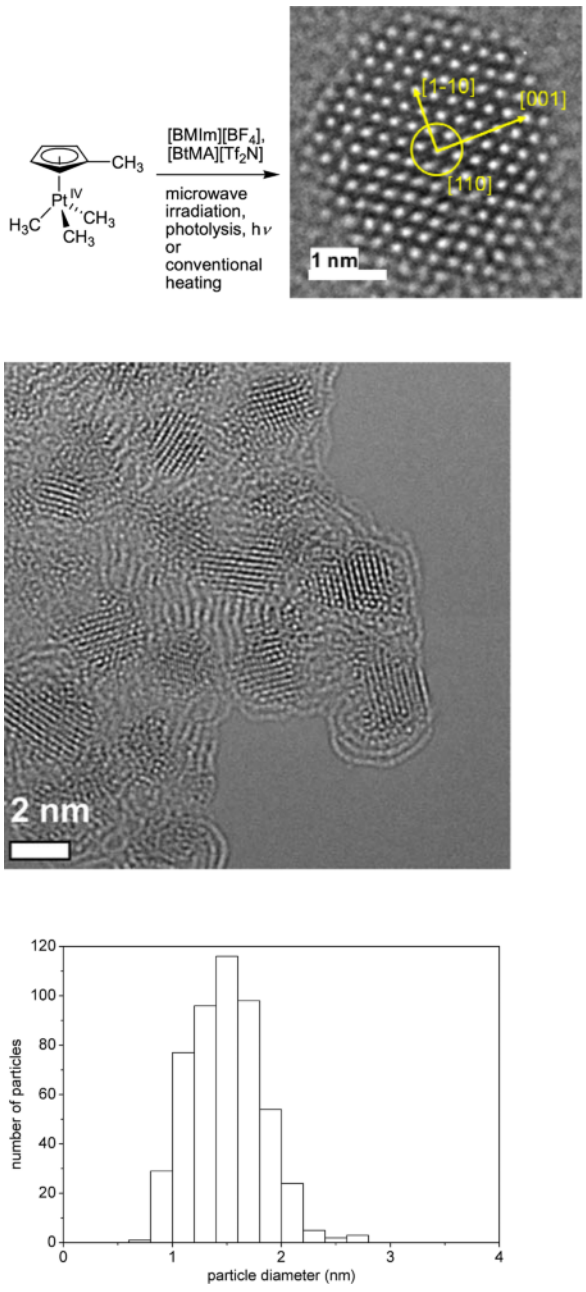

Fig. 8 (color online). Top: Growth of Pt-NPs shown in a high-resolution transmission electron microsopy (HR-TEM) picture of a single platinum nanocrystal viewed onto the {110} plane of the face-centered cubic unit cell (the bright spots are single Pt atoms). Middle: HR-TEM of several Pt-nanocrystals (showing the lattice planes) embedded in an IL matrix. Bottom: Histogram of Pt-NP diameter distribution (∅ 1.5 ± 0.5 nm, based on 505 particles) [117]. (In part reprinted from ref. [117] with permission from the author; © 2012 The Royal Society of Chemistry).

[HOEMIm][Tf_2N] gave smaller Pd-NPs with diameters 4.0 ± 0.6 nm compared with Pd-NPs isolated from the non-functionalized IL [BMIm][Tf_2N] with diameters 6.2 ± 1.1 nm [72]. Thermal reduction of $Pd(OAc)_2$ resulted in black NP solutions, and no precipitation of the NPs was observed over a period of several months. ^1H NMR spectra recorded before and after reduction of $Pd(OAc)_2$ showed no difference indicating that the alcohol group in the $[HOEMIm]^+$ cation is not the reductant [72].

Thermal, photolytic or microwave assisted decomposition of the air and moisture stable organometallic Pt(IV) precursor (MeCp)$PtMe_3$ in the ILs [BMIm][BF_4] and [BtMA][Tf_2N] leads to well defined, small, crystalline and longtime (> 7 months) stable Pt-nanocrystals without any additional reducing agents (Fig. 8). The Pt-NP/IL dispersion was shown to be a highly active catalyst (TOF 96 000 h^{-1} at 0.0125 mol.-% Pt and quantitative conversion) for the biphasic hydrosilylation of phenylacetylene with triethylsilane, to give the distal and proximal products triethyl(2- and 1-phenylvinyl)silane [117].

Pt nanoparticles generated from $H_2Pt(OH)_6$ and formic acid in [BMIm][FEP] (FEP = tris(pentafluoroethyl)trifluorophosphate) performed well in the chemoselective hydrogenation of 3-nitrostyrene with yields exceeding 90% to either 3-ethylnitrobenzene under acidic conditions or 3-aminostyrene under basic conditions (r. t., 1 bar H_2 pressure, TON ~ 100 h^{-1}). Immobilization on solid SiO_2 or carbon nanotube (CNTs) supports allowed for reuse [114].

The Ag-NP particle size distribution was very broad (several 10 nm or even 100 nm) when $AgBF_4$ was reduced with H_2 in the absence of the butyl-imidazole (BIm) scavenger. This can be explained with a perturbation of the IL matrix by the released protons (H^+) or acid (HBF_4) [140]. Also, the Ag-NP dispersion prepared without a scavenger is unstable as evidenced by clearly visible metal particle precipitation within 1 – 2 h after reduction. In the presence of the BIm scavenger and soluble silver salts the distribution of the Ag nanoparticles lies largely within 10 nm and the dispersion is stable up to 3 days under argon (Fig. 9) [80]. For these Ag-NPs a correlation between the IL anion molecular volume and the NP size was noted. The larger the volume of the IL anion, the larger is the size of the Ag-NPs. Thereby it was possible to form Ag-NPs in sizes from 2.8 to 26.1 nm with a narrow size distribution (Fig. 9) [80].

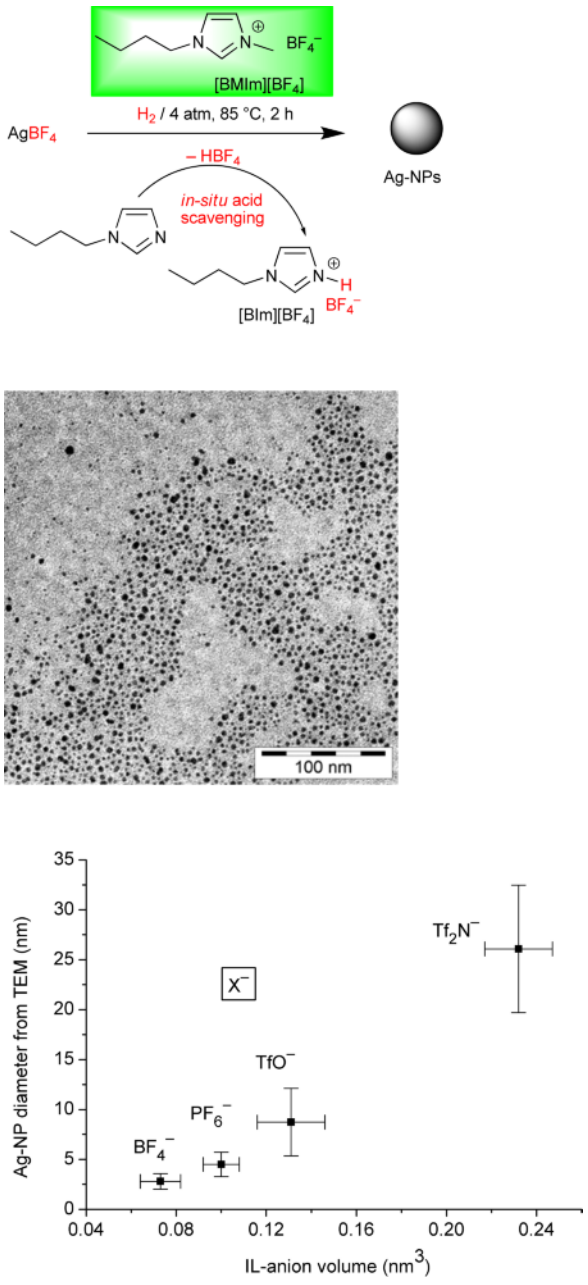

Fig. 9 (color online). Top: Formation of Ag-NPs (∅ 2.8 ± 0.8 nm) by hydrogen reduction of $AgBF_4$ with the concomitant imidazole scavenging in [BMIm][BF_4] (*cf.* Fig. 10). The ionic liquid formed from the scavenging process should be similar to the main IL solvent. Middle: TEM picture of Ag-NPs in [BMIm][BF_4]. Bottom: Correlation between the observed Ag nanoparticle size (from TEM) and the molecular volume of the ionic liquid anion (*cf.* Fig. 14) [80]. (TEM reprinted from ref. [80] with permission from the author; © 2008 American Chemical Society).

The synthesis and characterization of Au-NPs is of great interest due to their electronic, optical, thermal and catalytic properties associated with possible applications in the fields of physics, chemistry, biology, medicine, and material science [141]. Gold particles are among the best-studied particles in nano and materials science. A well-known method to generate Au-NPs was established by Turkevich *et al.* already in 1951 [142]. The reducing agent was citrate. By using this method the reduction could also be carried out in the imidazolium-based IL 1-ethyl-3-methylimidazolium ethylsulfate [EMIm][$EtSO_4$]. Afterwards it was possible to give these particles different shapes by adding a silver salt [143].

Also, cellulose is a reducing agent for Au(III) in $HAuCl_4$ and at the same time acts as a morphology- and size-directing agent, which drives the crystallization towards polyhedral particles or thick plates. The gold particle morphologies and sizes mainly depend on the reaction temperature. With this route plates with a thickness from 300 nm at 110 °C to 800 nm at 200 °C were synthesized [83].

By variation of the molar ratio of Au(III) to Sn(II) it was possible to synthesize Au-NPs in different sizes in a stop-and-go, stepwise and "ligand-free" nucleation and nanocrystal growth process which could be stopped and resumed at different color steps and Au-NP sizes from 2.6 to 200 nm. This stepwise Au-NP formation was possible because the IL apparently acted as a *kinetically* stabilizing, dynamic molecular network in which the reduced Au^0 atoms and clusters can move by diffusion and cluster together, as verified by TEM analysis [65].

Gold nanoparticles are also reproducibly obtained by thermal, photolytic or microwave-assisted decomposition/reduction under argon from Au(CO)Cl or $KAuCl_4$ in imidazolium-based ILs without an additional reducing agent. The reductive decomposition was carried out in the presence of *n*-butylimidazol as a scavenger (Fig. 10) dispersed in the ILs [BMIm][BF_4], [BMIm][TfO] or [BtMA][Tf_2N]. The ultra-small and uniform nanoparticles of about 1 – 2 nm diameter in [BMIm][BF_4] increase in size with the molecular volume of the ionic liquid anion in [BMIm][TfO] and [BtMA][Tf_2N]. Under argon the Au-NP/IL dispersion is stable without any additional stabilizers or capping molecules. In the ionic liquids the gold nanoparticles can be functionalized with organic thiol ligands, and transferred to and stabilized

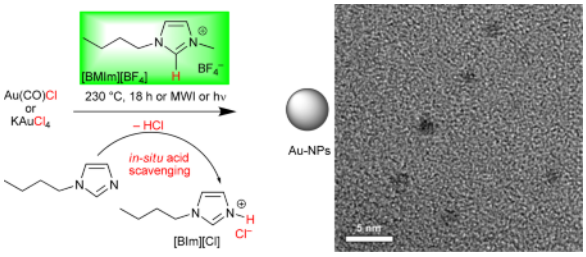

Fig. 10 (color online). Formation of Au-NPs (⌀ 1.1 ± 0.2 nm from $KAuCl_4$ in a thermal process) with the imidazole scavenging in [BMIm][BF_4] (*cf.* Fig. 8). The ionic liquid formed in the scavenging process should be similar to the main IL solvent [64]. The decomposition of Au(CO)Cl can also proceed by intramolecular reduction under formation of phosgene according to $2\,Au(CO)Cl \rightarrow 2Au + CO + COCl_2$ [144]. (TEM reprinted from ref. [64] with permission from the author; © 2011 Wiley-VCH).

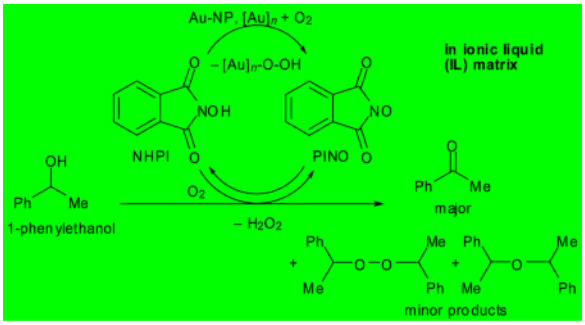

Fig. 11 (color online). Catalytic mechanism of the alcohol oxidation with Au-NP/IL/NHPI (NHPI + *N*-hydroxyphthalimide, PINO + phthalimide-*N*-oxyl radical) [146]. (Reprinted from ref. [146] with permission from the author; © 2011 Elsevier B. V.).

in different polar and non-polar organic solvents. Au-NPs can also be brought onto and stabilized by interaction with a polytetrafluoroethylene (PTFE, Teflon) surface [64].

Small Au-NPs of diameter 1.1 ± 0.2 nm, directly generated in the IL [BMIm][BF_4], can display quantized charges at room temperature. This phenomenon is well-known for nanoparticles that are protected by a strongly bound ligand shell, but could be demonstrated for naked metal clusters only in the special environment of an ionic liquid. DFT methods demonstrate that the cluster charging is accompanied by a switching in the orientation of the ionic shell [145].

Gold nanoparticles obtained by thermal reduction of $KAuCl_4$ in the presence of *n*-butyl-imidazol in [BMIm][BF_4] under nitrogen exhibited catalytic activities in the oxidation of 1-phenylethanol at 100 and 160 °C under 4 bar pressure of dioxygen in a base-free system (Fig. 11) [146]. Au-NP/IL in combination with the radical initiator *N*-hydroxyphthalimide (NHPI) showed good conversion and selectivity for the oxidation of 1-phenylethanol to acetophenone through formation of an α-hydroxy carbon radical. The concomitant side products di(1-phenylethyl)ether and di(1-phenylethyl)peroxide (Fig. 11) were rationalized by an equilibrium due to the IL matrix of the α-hydroxy carbon radical with the 1-phenylethoxy radical. Maximum turnover number was $\sim$ 5200 based on the total number of moles of gold but a factor of about six larger (TON $\approx$ 31 300) when considering only the Au-NP surface atoms. The fraction (N_S/N_T) of exposed surface atoms ($N_S \approx 2560$) for an average 8 nm Au-NP (having $N_T \approx 15\,800$ atoms in a $\sim$17-shell icosahedral or cuboctahedral particle) was estimated at 0.16 [146].

Au(I) and Au(III) salts ($KAuCN_2$ and $NaAuCl_4$, respectively), dissolved in [BMIm][PF_6], underwent reductive transformation to Au(0) to give gold nanoparticles which were found to be active catalysts for the cyclopropanation of alkenes with ethyldiazoacetate, in many cases affording high yields of cyclopropanecarboxylates. In ILs as solvents, the gold catalysts were stabilized, behaving as a metal nanoparticle reservoir, and products and catalyst separation and recycling could be achieved [147].

Carboxylic acid- and amino-functionalized ionic liquids [CMMIm][Cl] and [AEMIm][Br] (*cf.* Fig. 5) were used as stabilizers for the synthesis of gold and platinum metal nanoparticles in aqueous solution. Smaller Au-NPs (3.5 nm) and Pt-NPs (2.5 nm) were prepared with $NaBH_4$ as the reductant. Larger gold nanospheres (23, 42, and 98 nm) were synthesized using different quantities of trisodium citrate as a reductant. The morphology and the surface state of the metal nanoparticles were characterized by high-resolution transmission electron microscopy, UV/Vis spectroscopy, and X-ray photoelectron spectroscopy. X-Ray photoelectron spectra indicated that binding energies of C 1*s* and N 1*s* of the ionic liquids on the surface of metal nanoparticles shifted negatively compared with that of pure ionic liquids. The stabilization is proposed to be due to interactions between imidazolium ions/functional groups in the ionic liquids and metal atoms (*cf.* Fig. 6). The as-prepared metal nanoparticles could be easily assembled on mul-

tiwalled carbon nanotubes. In this case, ionic liquids acted as a linker to connect metal nanoparticles with carbon nanotubes. The imidazolium ring moiety of ionic liquids might interact with the π-electron system of the nanotube surface by virtue of cation-π and/or π-π interactions, and the functionalized group moiety of ionic liquids might interact with the metal-NPs surface (*cf.* Fig. 6c) [52].

Preparation of M-NP@support hybrid materials in ILs

The generation of M-NPs in ILs is also used to deposit the nanoparticles onto a support: Rhodium-NPs deposited on attapulgite (Rh-Atta) were prepared by immobilizing Rh^{3+} on Atta *via* the IL 1,1,3,3-tetramethyl-guanidinium lactate, followed by reduction with hydrogen at 300 °C. The rhodium loaded on Atta existed mainly in the form of Rh^0 with a small amount of its oxides and was distributed uniformly on Atta with a particle size of less than 5 nm. Atta was destroyed to some extent due to the impregnation by IL and Rh. The activity of the composite was investigated for cyclohexene hydrogenation and exhibited much higher efficiency compared to that of other catalysts, and the turnover frequencies reached 2700 (mol of cyclohexene per mol of Rh) per h [148]. For the deposition of Ru- and Rh-NPs from the metal carbonyl precursors onto a graphene derivative in IL matrix see Figs. 20 and 21 and accompanying text. The deposition of Rh-NPs from $Rh_6(CO)_{16}$ onto a Teflon surface using IL as a medium is illustrated in Fig. 23.

Uniform Pd nanoparticles supported on Vulcan XC-72 carbon were synthesized from H_2PdCl_4 and $NaBH_4$ using Guan-ILs (*cf.* Fig. 3) as a mediator for the nucleation and growth process [107].

Platinum nanoparticles synthesized by thermal decomposition of $(MeCp)PtMe_3$ in $[BMIm][BF_4]$ could be deposited on thiol-functionalized graphene derivatives (thermally reduced graphite oxide, TRGO) in the IL. The loading of Pt-NPs on thiol-functionalized TRGO ranged from 3.2 to 8.8 wt-% with particle diameters determined by TEM being 2.5 ± 0.9 to 9 ± 4 nm (Fig. 12) [149, 150].

Au-NP-decorated multiwalled carbon nanotube (MWCNT) hybrids (Au-MWCNT-HBs) were prepared by the ionic liquid-assisted sonochemical method (ILASM) on poly(ethylene terephthalate) (PET) films from $HAuCl_4 \cdot 3H_2O$, MWCNT and

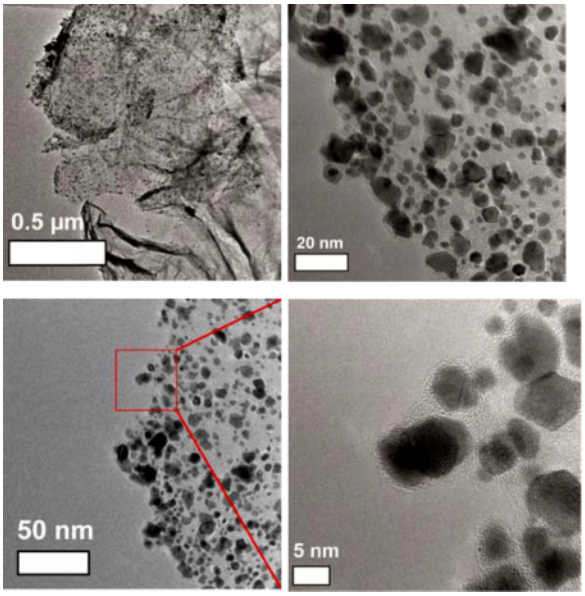

Fig. 12 (color online). HRTEM micrographs showing a section of Pt-NP-loaded flakes of thiol-functionalized graphene (thermally reduced graphite oxide) [149]. (Reprinted from ref. [149] with permission from the author; © 2013 Elsevier Ltd.).

$[BMIm][BF_4]$ [153]. Au-NPs can also be brought onto and stabilized by a polytetrafluoroethylene (PTFE, Teflon) surface [64].

An example of intermediate use of the IL is the synthesis of porous supported-nanoparticle materials by the encapsulation of poly(vinylpyrrolidone) (PVP)-stabilized Au-NPs into titania xerogels employing $[BMIm][PF_6]$ as a medium, followed by solvent extraction of the ionic liquid and calcination of the materials. The average Au-NP sizes increased from 5.5 ± 2.3 nm before to 8.8 ± 2.5 nm after calcination [151].

Photochemical reduction

Photochemical methods for the synthesis of M-NPs offer rather clean procedures because contaminations by reducing agents are excluded.

UV-induced decomposition of $(MeCp)PtMe_3$ was carried out in $[BMIm][BF_4]$ and $[BtMA][Tf_2N]$ to yield Pt-NPs of 1.1 ± 0.5 nm diameter when fresh (1 day old) and 1.7 ± 0.1 nm or 1.2 ± 0.4 nm when aged for 67 or 331 days, respectively [117].

A high-pressure mercury lamp was used to irradiate $AgClO_4$ in a mixture of an IL, water and Tween 20 (polyoxyethylene sorbitan monolaurate). Benzoin

was used as photoactivator. The average diameters of Ag-NPs prepared in water/[BMIm][BF_4] and water/[OMIm][BF_4] (1-octyl-3-methyl-imidazolium) microemulsions were 8.9 and 4.9 nm, respectively [152].

$HAuCl_4 \cdot 4H_2O$ in a mixed solvent of [BMIm][BF_4] and acetone (ratio 10 : 1) was irradiated for 8 h with UV light of a wavelength of 254 nm. The UV light turns the acetone into a free radical, which then reduces Au(III) to Au-NPs. The obtained Au nanosheets were about 4 μm long and 60 nm thick [90].

Au-NPs were formed from $HAuCl_4$ in the IL 1-decyl-3-methyl-imidazolium chloride in water when irradiated with 254 nm UV light for 30 to 70 min. The obtained nanorods had different shapes and morphologies. The sizes varied between 100 and 1000 nm [91].

Au-NPs are obtained by photolysis of Au(CO)Cl in [BMIm][BF_4] (*cf.* Fig. 10), albeit with large diameters of 61 ± 43 nm [64].

Sonochemical (ultrasound) reduction

$Pd(OAc)_2$ or $PdCl_2$ in the imidazolium-based ILs [BBIm][Br] or [BBIm][BF_4] were irradiated with ultrasound for 1 h. The Pd-NPs were nearly spherical and a size of 20 nm was observed. The formation of Pd biscarbene complexes as intermediates and their subsequent sonolytic conversion to Pd nanoparticles (*cf.* Fig. 7) have been established by NMR/MS and TEM analyses, respectively [88].

Au-NP-decorated MWCNT hybrids on PET films were prepared by ionic liquid-assisted sonication. The mixture of $HAuCl_4 \cdot 3H_2O$, MWCNT and [BMIm][BF_4] was sonicated for 60 s, resulting in the *in-situ* condensation of Au-NPs with narrow size distribution of 10.3 ± 1.5 nm decorated onto the surface of ionic liquid-wrapped MWCNTs [153]. Ultrasound was also used for the synthesis of ionic liquid-functionalized multiwalled carbon nanotubes decorated with highly dispersed Au nanoparticles from $HAuCl_4 \cdot 3H_2O$ in the presence of 1-(3-aminopropyl)-3-methyl-imidazolium bromide and dicyclohexylcarbodiimide albeit in DMF solution [154].

Electro(chemical) reduction

Ionic liquids have a high ionic conductivity, high thermal stability, negligible vapor pressure and a wide electrochemical window of up to 7 V which make them nearly inert in electrolytic processes. Electro-reduction is a clean route to prepare nanoparticles in ionic liquids as only electrons are used as the metal-reducing agent (see also the section on *Gas-phase synthesis – by plasma deposition methods, glow discharge (plasma) electrolysis*). It should be noted, however, that the size of the metal nanoparticles from electroreduction is often above the 100 nm definition limit for nanoparticles.

For the preparation of nanocrystalline metals a successful method is pulsed electrodeposition (PED) [155, 156]. This technique was used to deposit nano-Ni [157], nano-Pd [158], nano-Cu [159], nano-Fe [160], nano-Cr [161] and other metals with $E^0 > 0$ V as well as alloys like nano-Ni_xFe_{1-x} or nano-Ni_xCu_{1-x} [162] from aqueous electrolytes. Nanostructured less-noble metals like Al, Mg, W and their alloys cannot be electrodeposited from aqueous electrolytes but from ionic liquids [155]. For the electrodeposition of nano-Al the electrolyte may consist of [EMIm][Cl] and anydrous $AlCl_3$. Controlled nanostructures with crystallite sizes from 10 to 133 nm can be obtained with aromatic and aliphatic carboxylic acid additives, and their characteristics are also influenced by temperature [163]. Nanostructured iron was deposited from [BMIm][Cl], anhydrous $AlCl_3$ and $FeCl_3$ with benzoic acid as additive. The crystallite size of the nano-Fe deposits was adjusted to 40 – 160 nm by variation of the DC current density. The alloys Al_xMn_{1-x} and Al_xIn_{1-x} were deposited with crystallite sizes of 25 nm from [BMIm][Cl]/$AlCl_3$ with addition of the corresponding metal salts $MnCl_2$ and $InCl_3$, respectively [163].

CuCl as precursor was reduced in a cavity microelectrode in [BMIm][PF_6]. The electrode potential was varied. The smallest particles had a size of 10 nm and were obtained at an electrode potential of -1.8 V [164].

It is also possible to deposit metal particles on supporting material, *e. g.*, Ag-NPs from $AgBF_4$ in [BMIm][BF_4] on TiO_2. The electroreduction was performed in the high vacuum chamber of a SEM. The resulting Ag-NPs arranged themselves in a dendritic network structure [165]. The precursor Ag(TfO) was electrochemically reduced in [EMIm][TfO]. The prepared Ag nanowires were 3 μm long and 200 nm wide [166].

Polyaniline (PANI) and Au-NPs were synthesized as a composite material by cyclic voltammetry on a modified indium-tin-oxide (ITO) glass in the IL 1-ethyl-3-methyl-imidazolium tosylate [EMIM][Tos]

containing 1 mol L^{-1} trifluoroacetic acid. The Au particles were synthesized during electropolymerization of aniline and distributed in the PANI matrix. SEM showed that Au particles with diameters in the range from 500 to 800 nm were distributed in the PANI matrix [167].

Graphene oxide (GO) and $HAuCl_4$ were simultaneously reduced in [BMIm][PF_6] at a potential of −2.0 V. The obtained Au-NPs on the electrochemically reduced graphene had a size of 10 nm [168].

Morpholinium ionic liquid, [BMMor][BF_4]-stabilized palladium (Pd) nanoparticles were prepared by electrochemical reduction using a palladium foil as the anode and a platinum foil as the cathode. Pd ions released from the Pd anode migrated to the Pt cathode and there Pd ions were reduced to Pd atoms forming the nanoparticles. The particle size increased with a decrease in the current density and an increase in temperature and electrolysis duration. TEM images showed average sizes of 2.0 ± 0.1, 2.2 ± 0.3, 2.4 ± 0.3, 2.9 ± 0.3, 3.5 ± 0.5, 3.9 ± 0.6, and 4.5 ± 0.9 nm. Nearly a 0.5 nm-size control of the nanoparticle was achieved. The electron diffraction patterns of the resulting nanoparticles indicated that the particles had a crystalline structure [169].

Gas-phase synthesis

Gas-phase synthesis is most effective for high purity nanoparticle products. Gas-phase synthesis methods can be discerned in gas-phase condensation and flame pyrolysis. In the gas-phase condensation, the metal is vaporized from heated crucibles, by electron or laser beam evaporation or sputtering and condensed onto a liquid, here an IL. When the metal as the evaporative source is replaced with a precursor compound for decomposition, then the gas-phase condensation is termed a chemical vapor condensation or chemical vapor synthesis. For flame pyrolysis, the gaseous or liquid precursors are decomposed by a combustion reaction [170]. The negligible vapor pressure of (room temperature) ILs allows to introduce RT-ILs in methods requiring vacuum conditions. For metal nanoparticle synthesis, such methods are magnetron sputtering onto ILs, plasma reduction in ILs, physical vapor deposition onto ILs, and electron beam and γ-irradiation of ILs. The nanoparticles prepared in ILs without any stabilizing agent do not aggregate in the ILs [33].

– by magnetron sputtering

Sputtering of clusters or atoms onto ILs to yield nanoparticles therein is possible for all elements that can be ejected from a target by Ar^+ and N_2^+ plasma ion bombardment. This method has yielded various pure metal nanoparticles, such as Au, Ag, Pt and others with particle sizes less than 10 nm in diameter and without any specific stabilizing agent. Both surface tension and viscosity of the IL are important factors for the nanoparticle growth and stabilization [33].

Sputter deposition of indium in the ionic liquids [BMIm][BF_4], [EMIm][BF_4], [(1-allyl)MIm][BF_4] and [(1-allyl)EIm][BF_4] produced stable In metal nanoparticles whose surface was covered by an amorphous In_2O_3 layer to form In/In_2O_3 core/shell particles. The size of the In core was tunable from *ca.* 8 to 20 nm by selecting the IL [171].

Pt nanoparticles were produced by Pt sputtering onto the IL trimethyl-*n*-propylammonium bis((trifluoromethyl)sulfonyl)amide [Me_3PrN][Tf_2N] without stabilizing agents. The Pt nanoparticles showed mean particle diameters of *ca.* 2.3 – 2.4 nm independent of sputtering time [172]. By using these Pt-sputtered ILs the Pt-NP immobilization onto single-walled carbon nanotubes to yield Pt-NP-SWCNT composites was achieved without any pretreatment of SWCNTs or any chemical reagent [173].

Gold nanoparticles of 1 – 4 nm size could be prepared by sputter deposition of the metal onto the surface of the ionic liquid [BMIm][BF_4] to generate nanoparticles in the liquid with no additional stabilizing agents [174]. Likewise, Au-NPs were prepared by sputter deposition of Au metal in [BMIm][PF_6]. The size of Au nanoparticles was increased from 2.6 to 4.8 nm by heat treatment at 373 K [175].

Au-NPs with the size of 3 to 5 nm were obtained with gold foil by sputtering deposition onto several imidazolium-based ILs [176].

– by plasma deposition, glow discharge (plasma) electrolysis

When a gas is partially ionized, becomes electrically conductive and has collective behavior it is called a plasma. Plasma deposition, once known as glow discharge electrolysis (GDE) [33] is an electrochemical technique in which the discharge is initiated in the gas in between the metal electrode and the solution by

Table 2. Nanoparticles by plasma deposition method (glow discharge plasma electrolysis) in ILs.

Metal	Metal precursor	Ionic liquid[a]	Average particle diameter ± standard deviation (nm)	Ref.
Pd	$PdCl_2$	[BMIm][BF_4]	32.7	[179]
Cu	$Cu(TfO)_2$	[BMPy][TfO]	~40, deposited on gold surface	[180]
	Cu	[EMIm][Tf_2N]	~11	[181]
	Cu	[BMPy][Tf_2N]	~26	[181]
Ag	$AgNO_3$/Ag(TfO)	[BMIm][TfO]	~8 – 30	[170, 182]
	Ag(TfO)	[EMIm][TfO]	20	[170, 180]
	$AgBF_4$	[BMIm][BF_4], [BMIm][PF_6]	<100, at glassy carbon electrode	[183]
Au	$HAuCl_4$	[BMIm][BF_4]	~2	[177]
	$HAuCl_4 \cdot 4H_2O$	[BMIm][BF_4]	1.7 ± 0.8	[184]
Al	$AlCl_3$	[BMPy][Tf_2N]	~34, 20 – 64, deposited on gold surface	[180]
Ge	$GeCl_2$ dioxane	[EMIm][Tf_2N]	<50	[185]

[a] For non-functionalized ILs, see Fig. 3, for functionalized ILs, see Fig. 5.

applying high voltage. In ionic liquid glow discharge electrolysis (IL-GDE) the discharge is initiated in the gas in between the metal electrode and the ionic liquid solution. The technique is also named plasma electrochemical deposition (PECD) [155, 156, 170] at the interface of plasma and ionic liquid, or gas-liquid interfacial discharge plasmas (GLIDPs) [177]. The plasma is regarded as an electrode because of the deposition of the materials at the interface of ionic liquid and plasma. In IL-GDE the precursor material dissolved in IL is reduced with free electrons from the plasma [170, 178]. Table 2 summarizes metal nanoparticles which were obtained by IL-GDE.

Gold nanoparticle-DNA encapsulated single-walled carbon nanotubes (SWNTs) were generated using GLIDP by superimposing a DC voltage to the pulse voltage, where the IL containing DNA and $HAuCl_4$ is used as the liquid electrode [177].

A sub-atmospheric dielectric barrier discharge (SADBD) plasma was used for the reduction of $HAuCl_4 \cdot 4H_2O$ to Au-NPs. By introducing polyvinylpyrrolidone (PVP) as a capping agent, the nanoparticle diameter was controlled to ~ 1.7 nm with a narrow size distribution [184].

– by physical vapor deposition

This method is based on a solvated metal atom dispersion technique. It offers an easy and fast method for the preparation of long-term-stable metal and metal-oxide particles. The use of ILs avoids the otherwise needed freezing of the solvent as well as additional stabilizers [186].

Evaporation of elemental Cu powder under high vacuum (10^6 Torr) on the surface of [BMIm][PF_6] or [BMIm][Tf_2N] generated Cu nanoparticles with a mean diameter of 3 nm [186]. Cu-NPs generated in [BMIm][Tf_2N] with 3.7 ± 1.2 nm grew to 5 ± 2 nm after 45 min at 50 °C [187]. Cu metal was also vaporized into an IL dispersion of ZnO to give Cu-NPs with ~ 3.5 nm diameter on or near the ZnO surface [186].

Gas-phase deposition from metal vaporization on the surface of ILs gave Au-NPs whose average diameter (∅) depended on the IL: [BMIm][BF_4] ∅ 7 nm, [BMIm][Tf_2N] ∅ 4 nm, [BMPy][Tf_2N] ∅ 20 – 40 nm, [BMIm][DCA] (DCA = dicyanamide) initially ∅ 10 nm, later 40 – 80 nm, and [P_{66614}][DCA] (P_{66614} = trihexyl(tetradecyl)phosphonium) ∅ 50 nm [186]. In a follow-up study Au-NPs of mean particle diameter of 2.7 ± 1.4 nm in [BMIm][Tf_2N] and 2.7 ± 0.6 nm in [BMIm][PF_6] were prepared [187]. These as-prepared particle sizes grow to 5.5 ± 1.5 nm and 3.3 ± 0.7 nm after 45 and 120 min at 50 °C, respectively, in a ripening process. In [BMIm][PF_6] the Au-NPs reached 4.3 ± 0.9 nm after 20 h at 50 °C. The final size seemed to be independent of the concentration of metal and the bulk properties of the IL, but dependent on the chemical identity of the IL

Table 3. Binary metal carbonyls[a].

Group	**5**	**6**	**7**	**8**	**9**	**10**
Metal	**V, Nb, Ta**	**Cr, Mo, W**	**Mn, Tc, Re**	**Fe, Ru, Os**	**Co, Rh, Ir**	**Ni, Pd, Pt**
Mono-nuclear complexes	$V(CO)_6$	**$Cr(CO)_6$** **$Mo(CO)_6$** **$W(CO)_6$**		**$Fe(CO)_5$** $Ru(CO)_5$ $Os(CO)_5$		**$Ni(CO)_4$**
Poly-nuclear complexes			**$Mn_2(CO)_{10}$** $Tc_2(CO)_{10}$ **$Re_2(CO)_{10}$**	**$Fe_2(CO)_9$** **$Fe_3(CO)_{12}$** $Ru_2(CO)_9$ **$Ru_3(CO)_{12}$** $Os_2(CO)_9$ **$Os_3(CO)_{12}$**	**$Co_2(CO)_8$** **$Co_4(CO)_{12}$** **$Rh_4(CO)_{12}$** **$Rh_6(CO)_{16}$** **$Ir_4(CO_{12}$**	

[a] Metal carbonyls given in bold are commercially available, *e. g.*, from Aldrich, ABCR or Acros.

matrix. Short alkyl chain-length methyl-imidazolium salts with weakly coordinating perfluorinated counter anions (BF_4, PF_6 or Tf_2N) appeared to be better stabilizers than ILs with alkyl chain cations such as tris(hexyltetradecyl)phosphonium or 1-octyl-3-methyl-imidazolium and better coordinating anions (*e. g.* dicyanamide). In the latter ILs, fast particle growth and agglomeration was observed [187].

– by electron beam and γ-irradiation

Very strong electron beam and γ-irradiation of the ILs containing metal salts yield solvated electrons and/or radicals through which metal nanoparticles are then generated [33].

$NaAuCl_4 \cdot 2H_2O$ gave Au-NPs after accelerator electron beam and γ-irradiation both at 6 kGy and 20 kGy in [BMIm][Tf_2N]. By accelerator electron beam irradation spherical Au nanoparticles were formed with a mean particle diameter of 7.6 ± 1.5 nm at 6 kGy irradiation and of 26.4 ± 3.7 nm at 20 kGy. The γ-irradiation method produces smaller Au nanoparticles with 2.9 ± 0.3 nm and 10.7 ± 1.7 nm at 6 kGy and 20 kGy, respectively, in [BMIm][Tf_2N]. It was emphasized that the prepared Au-NPs were stable without the need for a stabilizing additive for more than three months [188].

A low-energy electron beam irradiation was used to synthesize Au-NPs from the $NaAuCl_4 \cdot 2H_2O$ precursor in the IL [BMIm][Tf_2N]. The obtained particles had a large size of 122 nm [189].

Metal nanoparticles from zero-valent metal precursors

Metal nanoparticles from metal carbonyls, $M_x(CO)_y$

The use of binary metal carbonyls for the synthesis of metal nanoparticles is sensible and logical. Metal carbonyls are commercially available (Table 3). $Fe(CO)_5$ and $Ni(CO)_4$ are industrially produced on a multi-ton scale [190]. Compounds $M_x(CO)_y$ can be easily purified and handled, even if care should be exerted for the possible liberation of poisonous CO. The metal carbonyls contain the metal atoms already in the zero-valent oxidation state needed for M-NPs. No reducing agent is necessary. The side product CO is largely given off to the gas phase and removed from the dispersion. Contamination with by- or decomposition products, which are otherwise generated during the M-NP synthesis, is greatly reduced. Thus, metal carbonyls were used early on for the preparation of M-NPs, albeit without ILs, with much of the work on Fe- or Co-NPs being devoted to magnetism [191].

The M-NP synthesis in IL from $M_x(CO)_y$ is generally carried out without any additional stabilizers, surfactants or capping molecules. Metal carbonyls can be decomposed to metal nanoparticles in ILs by conventional heating, UV photolysis or microwave irradiation (MWI) (Fig. 13a–c, Table 4).

Ionic liquids are an especially attractive medium for microwave reactions. They efficiently absorb microwave energy due to their ionic character with high polarity, high polarizability and high dielectric constant. Consequently ILs show a high dissipation factor (tan δ) for the conversion of microwave energy into heat [34, 192]. Microwaves are a low-frequency energy source which can be used for many chemical reactions [34, 193 – 195]. Microwave radiation directly heats the reaction mixture and not the vessel, *i. e.*, it is the reaction mixture which absorbs the microwave energy. This leads to localized superheating, very fast and efficient heating rates so that temperatures of 200 °C are reached within seconds [193, 196 – 198]. As soon as metal particles have formed from the decomposition of the precursor, they can also absorb the microwave

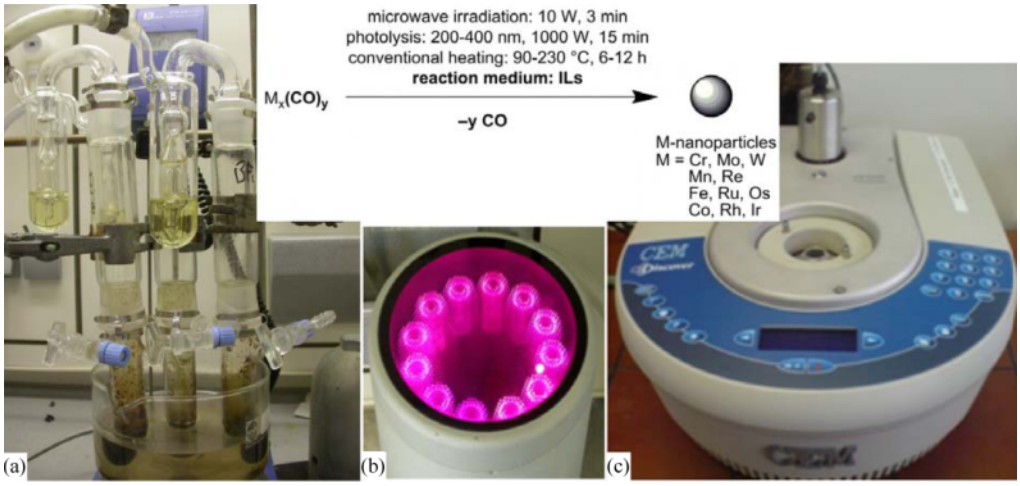

Fig. 13 (color online). (a) Setup for conventional thermal decomposition of $M_x(CO)_y$/IL dispersions under argon, (b) UV reactor, (c) commercial laboratory microwave reactor [30]. (Reprinted from ref. [30] with permission from the author; © 2011 Elsevier B. V.).

Table 4. Examples of M-NPs prepared in ILs from metal carbonyls.

Metal	Metal carbonyl precursor	Ionic liquid[a]	M-NP average diameter ± standard deviation (nm)	Remarks	Ref.
Monometallic					
Cr	$Cr(CO)_6$	[BMIm][BF_4], [BMIm][TfO], [BMIm][Tf_2N]	≤ 1.5 ± 0.3, MWI, thermal;[b] 4.4 ± 1.0, hν[b]	[c,d,e,f] see Fig. 15	[85, 95]
	$Cr(CO)_6$	[EMIm]Cl	3.6 ± 0.7 nm, MWI, 2.3 ± 0.4 nm, thermal	cat. for glucose to HMF conversion, see Fig. 17	[207]
Mo	$Mo(CO)_6$	[BMIm][BF_4], [BMIm][TfO], [BMIm][Tf_2N]	~1 – 2, MWI, hν;[b] ≤ 1.5 ± 0.3, thermal[b]	[c,d,e,f]	[85, 95]
W	$W(CO)_6$	[BMIm][BF_4], [BMIm][TfO], [BMIm][Tf_2N]	3.1 ± 0.8, MWI;[b] <1, hν;[b] ≤ 1.5 ± 0.3, thermal[b]	[c,d,e,f] see Fig. 14	[85, 95]
Mn	Mn_2CO_{10}	[BMIm][BF_4]	12.4 ± 3, MWI; <1, hν 28.6 ± 11.5, MWI	[b,c,d] see Fig. 15	[85] [78]
	Mn_2CO_{10}	[CEMIm][BF_4]	4.3 ± 1.0, MWI	see text	[78]
Re	Re_2CO_{10}	[BMIm][BF_4]	2.4 ± 0.9, MWI; <1, hν	[c,d,e] see Fig. 16	[85]
Fe	$Fe_2(CO)_9$	[BMIm][BF_4]	8.6 ± 3.2, MWI;[b] 7.0 ± 3.1, hν;[b] 5.2 ± 1.6, thermal[b]	[c,d,e,f]	[23, 85]
	$Fe_2(CO)_9$	[BMIm][PF_6]	thermal	cyclohexenone hydrogenat. cat.	[208]
Ru	$Ru_3(CO)_{12}$	[BMIm][BF_4]	1.6 ± 0.3, MWI;[b] 2.0 ± 0.5, hν;[b] 1.6 ± 0.4, thermal[b]	[c,d,e,f]; see Fig. 16, hydrogenation cat., *cf.* Fig. 18	[23, 85]
	$Ru_3(CO)_{12}$	[BMIm][BF_4]	2.2 ± 0.4, MWI	Ru-NPs deposited on TRGO, see text, Figs. 20 – 22	[224]

Table 4. Continued.

Metal	Metal carbonyl precursor	Ionic liquid[a]	M-NP average diameter ± standard deviation (nm)	Remarks	Ref.
	$Ru_3(CO)_{12}$	[BMIm][PF_6]	2.9 ± 0.8, thermal	cyclohexenone hydrogenat. cat.	[208]
Os	$Os_3(CO)_{12}$	[BMIm][BF_4]	0.7 ± 0.2, MWI;[b] 2.0 ± 1.0, hν;[b] 2.5 ± 0.4, thermal	[c,d,e,f]	[23, 85]
Co	$Co_2(CO)_8$	[BMIm][BF_4], [BMIm][TfO], [BMIm][Tf_2N]	5.1 ± 0.9, MWI;[b] 8.1 ± 2.5, hν;[b] 14 ± 8, thermal[b]	[c,d,e,f]	[23, 85]
	$Co_2(CO)_8$	[CEMIm][BF_4]	1.6 ± 0.3, MWI	see text	[78]
	$Co_2(CO)_8$	[C_xMIm][Tf_2N]	7.7, thermal at 150 °C	Fischer-Tropsch catalyst giving olefins, oxygenates, and paraffins (C_7–C_{30}), reusable at least three times	[209]
	$Co_2(CO)_8$	[C_{10}MIm][Tf_2N]	53 ± 22, thermal at 150 °C	Co-NPs with cubic shape together with Co-NPs of irregular shape	[210]
	$Co_2(CO)_8$	[Oct_3MA] [BMPy][Tf_2N], [BMIm][PF_6], [BMIm][Tf_2N], [BMIm][BF_4]	5.8 ± 0.9 to 16 ± 3 3.6 ± 0.7 to 21 ± 6 6 ± 1 to 7 ± 1 11 ± 3 4 ± 2	magnetic fluids, size varies with concentration,	[211]
Rh	$Rh_6(CO)_{16}$	[BMIm][BF_4], [BMIm][TfO], [BMIm][Tf_2N]	1.7 ± 0.3, MWI;[b] 1.9 ± 0.3, hν;[b] 3.5 ± 0.8, thermal[b]	[c,d,e,f]; see Fig. 14 hydrogenation cat., *cf.* Figs. 19 and 22	[23, 85]
	$Rh_6(CO)_{16}$	[BMIm][BF_4]	2.8 ± 0.5	Rh-NPs deposited on TRGO, see text, Figs. 20 – 22	[224]
	$Rh_6(CO)_{16}$	[BMIm][BF_4]	2.1 ± 0.5	Rh-NPs deposited on Teflon-coated stirring bar, see text, Fig. 23	[212]
Ir	$Ir_4(CO)_{12}$	[BMIm][BF_4], [BMIm][TfO], [BMIm][Tf_2N]	0.8 ± 0.2, MWI;[b] 1.4 ± 0.3, hν;[b] 1.1 ± 0.2, thermal[b]	[c,d,e,f]; hydrogenation catalyst	[23, 85]
Bimetallic					
FeRu 1 : 1	$Fe_2(CO)_9$, $Ru_3(CO)_{12}$	[BMIm][PF_6]	1.7 ± 0.3, thermal	cyclohexenone hydrogenat. cat.	[208]

[a] For non-functionalized ILs, see Fig. 3, for functionalized ILs, see Fig. 5; [b] in [BMIm][BF_4]; [c] median diameters and standard deviations are from TEM measurements; [d] microwave decomposition of metal carbonyls with 10 W for 3 – 10 min; [e] photolytic decomposition of metal carbonyls with a 1000 W Hg lamp (200 – 450 nm wavelength) for 15 min; [f] thermal decomposition of metal carbonyls for 6 – 12 h at 180 – 230 °C depending on the metal carbonyl.

radiation. Theoretical calculations have indicated that due to their high surface-to-volume ratio nanoscopic (metallic or magnetic) particles quickly reach a thermal stationary state upon electromagnetic excitation with negligible temperature difference between the volume phase of the particle and its surrounding. Depending on particle size and surrounding medium initiation times around 100 ps are expected [199 – 201]. Experimental findings suggest further that the energy transfer between particle and the surrounding phase

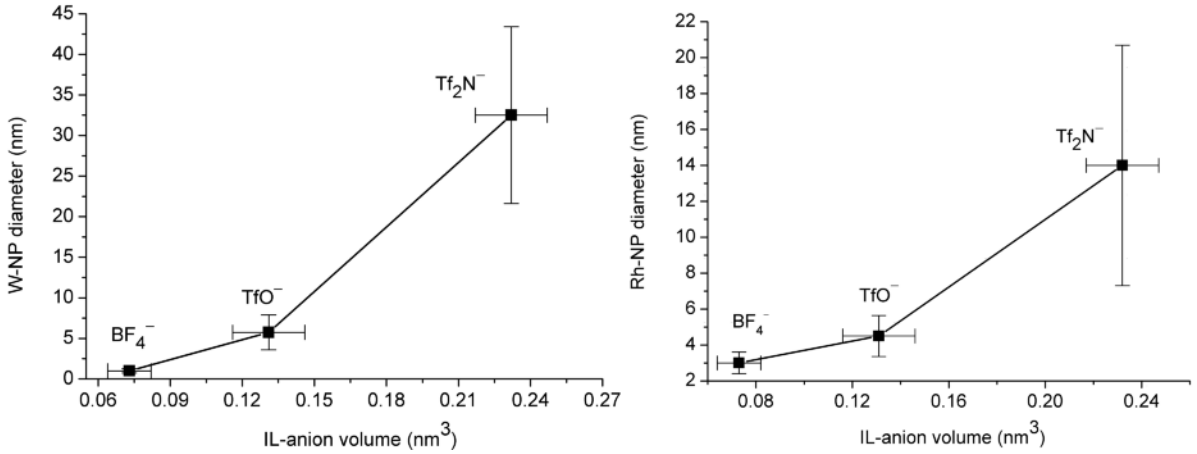

Fig. 14. Correlation between the molecular volume of the ionic liquid anion and the observed W and Rh nanoparticle size with standard deviations as error bars (from TEM, *cf.* Fig. 9) [95, 96]. (Adapted from ref. [30] with permission from the author; © 2011 Elsevier B. V.).

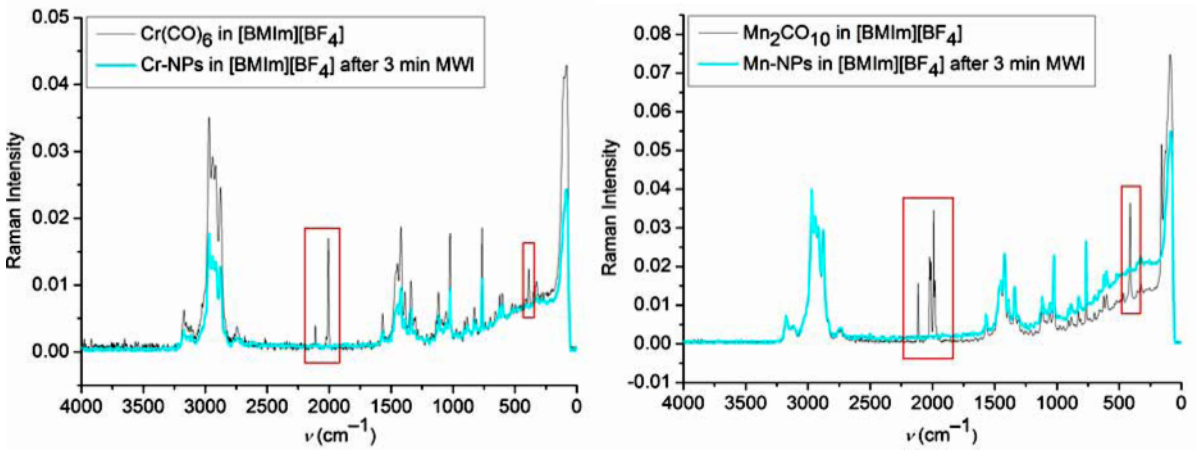

Fig. 15 (color online). Raman-FT spectra. $Cr(CO)_6$ and $Mn_2(CO)_{10}$ in [BMIm][BF_4] before and after 3 min 10 W microwave irradiation (MWI). Red boxes highlight the relevant metal carbonyl bands [30, 85]. (Reprinted from ref. [30] with permission from the author; © 2011 Elsevier B. V.).

leads to increased excitation of vibrational degrees of freedom in surface-bound or surface-near molecules which can in turn be used for the activation of reactions. Any presumptions about abnormal "microwave effects" [202 – 204] have been proven wrong in the meantime [205, 206]. Moreover, microwave reactions are also an "instant on/instant off" energy source, significantly reducing the risk of overheating [193, 196].

Metal nanoparticles (M-NPs) were reproducibly obtained from their metal carbonyl precursors $M_x(CO)_y$ in ILs by easy, rapid (few minutes) and energy-saving (as low as 10 Watt) microwave irradiation (MWI) under an argon atmosphere. This MWI synthesis was compared to UV-photolytic (1000 W, 15 min) or conventional thermal decomposition (180 – 250 °C, 6 – 12 h) of $M_x(CO)_y$ in ILs. The MWI-obtained nanoparticles have a very small (< 5 nm) and uniform size and are prepared without any additional stabilizers or capping molecules as long-term stable M-NP/IL dispersions [30, 85].

For W- and Rh-NPs it was shown that the diameter increases with the molecular volume of the ionic liquid anion (Fig. 14) [95, 96].

Complete $M_x(CO)_y$ decomposition by the short, 3 – 10 min microwave irradiation was verified by Raman spectroscopy with no (metal-)carbonyl bands be-

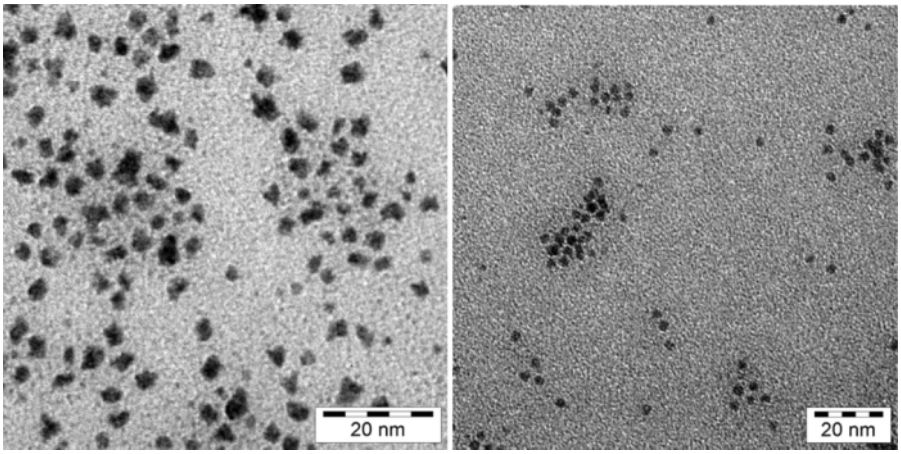

Fig. 16. TEM photographs. Left: Re-NPs from $Re_2(CO)_{10}$ by MWI, ∅ 2.4 ± 0.9 nm. Right: Ru-NPs from $Ru_3(CO)_{12}$ by photolytic decomposition, ∅ 2.0 ± 0.5 nm (*cf.* Table 4) [30, 85]. (Reprinted from ref. [85] with permission from the author; © 2010 Wiley-VCH).

tween 1750 and 2000 cm^{-1} being observed any more after the microwave treatment (Fig. 15) [30, 85].

Examples of TEM pictures of metal nanoparticles obtained by microwave irradiation or UV photolysis of their metal carbonyl precursors $M_x(CO)_y$ in [BMIm][BF_4] are given in Fig. 16 [85].

The synthesis of Co-NPs and Mn-NPs by microwave-induced decomposition of the metal carbonyls $Co_2(CO)_8$ and $Mn_2(CO)_{10}$, respectively, yields smaller and better separated particles in the functionalized IL 1-(3-carboxyethyl)-3-methylimidazolium tetrafluoroborate [CEMIm][BF_4] (1.6 ± 0.3 nm and 4.3 ± 1.0 nm, respectively) than in the non-functionalized IL [Bmim][BF_4] (see Table 4). The particles are stable in the absence of capping ligands (surfactants) for more than six months although some variation in particle size could be observed by TEM [78].

Metal nanoparticles from zero-valent metal precursors other than $M_x(CO)_y$

Copper nanoparticles were easily obtained by stirring 1 – 5 μm copper particles in [BMIm][NO_3] for 5 h with an IL/Cu flake weight ratio of 1 : 0.02. Cu-NPs did hardly form at this weight ratio when [BMIm][BF_4] or [BMIm][PF_6] were used as ILs [213].

Zero-valent organometallic compounds available include [Ru(COD)(COT)] and [$Ni(COD)_2$] (COD = 1,5-cyclooctadiene, COT = 1,3,5-cyclooctatriene). Hydrogen as a reagent was used to hydrogenate the ligands COD and COT to cyclooctane which was subsequently lost from the Ru(0) or Ni(0) metal atom [86, 97, 98, 214]. [Ru(COD)(COT)] or [$Ni(COD)_2$] were dissolved in imidazolium based ILs and the mixture heated under 4 bar of hydrogen under different conditions to obtain metal nanoparticles (Table 5). Cyclooctane could then be removed under reduced pressure.

Ruthenium nanoparticles Ru-NPs were obtained by decomposition, under H_2, of (η^4-1,5-cyclooctadiene)(η^6-1,3,5-cyclooctatriene)ruthenium(0), [Ru(COD)(COT)], in various 1-alkyl-3-methyl-imidazolium ionic liquids ([C_xMIm][Tf_2N] ($C_x = C_nH_{2n+1}$ where $n = 2$; 4; 6; 8; 10), and [BBIm][Tf_2N] and [BMMIm][Tf_2N] ([BMMIm]$^+$ = 1-butyl-2,3 dimethyl-imidazolium). The synthesis has been performed under 0.4 MPa of H_2, at 25 °C or at 0 °C with or without stirring. A relationship between the size of IL non-polar domains calculated by molecular dynamics simulation and the Ru-NP size measured by TEM has been found. This suggested that the crystal growth is probably controlled by the local concentration of [Ru(COD)(COT)] and consequently is limited to the size of the non-polar domains [215]. The size of ruthenium nanoparticles is governed by the degree of self-organization of the imidazolium based ionic liquid in which they are generated: the more structured the ionic liquid, the smaller the size [97]. The stabilization of Ru-NPs in imidazolium ILs is related to the presence of surface hydrides and their confinement in non-polar domains due to the continuous 3-D network of ionic channels [216].

Table 5. Examples of M-NPs prepared in ILs from zero-valent metal precursors other than metal carbonyls.

Metal	Metal precursor[a]	IL[a]	M-NP diameter ± standard deviation (nm)	Ref.
Cu	1 – 5 μm Cu flakes	[BMIm][NO_3]	10	
Ru	[Ru(COD)(COT)][b]	[BMIm][Tf_2N]	0.9 – 2.4	[97]
		[BMIm][Tf_2N] with H_2O or 1-octylamine (OA)	H_2O: ~ 2 nm NPs grouped in circular aggregates of 20 – 30 nm; OA with OA/Ru >0.1: 1.1 ± 0.3	[98]
		[BMIm][BF_4], [BMIm][PF_6], [BMIm][TfO]	2.6 ± 4	
Ni	[$Ni(COD)_2$][b]	[C_xMIm][Tf_2N]	4.9 ± 0.9 to 5.9 ± 1.4	[86]

[a] For non-functionalized ILs, see Fig. 3, for functionalized ILs, see Fig. 5; [b] COD = 1,5-cyclooctadiene, COT = 1,3,5-cyclooctatriene.

Very stable suspensions of small (*ca.* 1.2 nm) and homogeneously dispersed Ru-NPs were obtained under H_2 from [Ru(COD)(COT)], in the above imidazolium ionic liquids ([C_xMIm][Tf_2N] and in the presence of amines as ligands (1-octylamine, 1-hexadecylamine). NMR experiments (^{13}C solution and DOSY) demonstrated that the amines are coordinated to the surface of the Ru-NPs. These Ru-NPs were investigated as catalysts for the hydrogenation of aromatics and have shown a high level of recyclability (up to 10 cycles) with neither loss of activity nor significant agglomeration [217].

By thermal decomposition of bis(1,5-cyclooctadiene)nickel(0), [$Ni(COD)_2$], nickel nanoparticles were prepared in 1-alkyl-3-methyl-imidazolium bis-(trifluoromethylsulfonyl)amide ionic liquids [86].

Catalytic applications of metal nanoparticles derived from $M_x(CO)_y$

In the absence of strongly coordinating protective ligand layers, metal nanoparticles in ILs should be effective catalysts. The IL network contains only weakly coordinating cations and anions (see Fig. 3) that bind less strongly to the metal surface and, hence, are less deactivating, than the commonly employed capping or protective ligands. The combination of M-NPs and ILs can be considered a *green catalytic* system because it can avoid the use of organic solvents. ILs are interesting in the context of green catalysis [218] which requires that catalysts be designed for easy product separation from the reaction products and multi-time efficient reuse/recycling [34, 219, 220]. Firstly, the very low vapor pressure of the IL and designable low miscibility of ILs with organic substrates allows for a facile separation of volatile products by distillation or removal in vacuum. Secondly, the IL is able to retain the M-NPs for catalyst reuse and recycling. M-NP/IL systems were shown to be quite easily recyclable and reusable several times without any significant changes in catalytic activity [25]. In hydrogenation reactions with Rh- or Ru-NP/IL systems the catalytic activity did not decrease upon repeated reuse [85, 96]. A sizable number of catalytic reactions have successfully been carried out in ILs [10, 12, 221]. Generally, the catalytic properties (activity and selectivity) of dispersed M-NPs indicate that they possess pronounced surface-like (multi-site) rather than single-site-like character [222, 223]. Fe- [13], Ru- [14], Rh- [15] and Ir-NPs [16] have been the subject of reviews concerning their synthesis, stabilization and size-control by various methods and also in different ILs, followed by a survey of their catalytic activity in organic hydrogenation [13, 15, 16], hydroformylation [15] and cross-coupling [13] reactions, in multiphase conditions [14, 15] and in energy-related processes such as biomass refinement [14].

Cr-NPs from $Cr(CO)_6$ were effective for the conversion (dehydration) of glucose to 5-hydroxymethylfurfural (HMF) (Fig. 17) in the IL [EMIm]Cl at $T = 120$ °C [207].

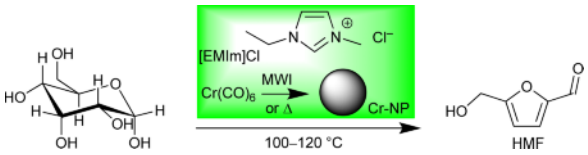

Fig. 17 (color online). Conversion of glucose to 5-hydroxymethylfurfural (HMF) by Cr-NPs (obtained from $Cr(CO)_6$). Carbonyl complexes $Mn_2(CO)_{10}$, $Fe(CO)_5$, $Fe_2(CO)_9$ and $Co_2(CO)_8$ and Mn-, Fe- or Co-NPs derived therefrom did not catalyze this conversion [207].

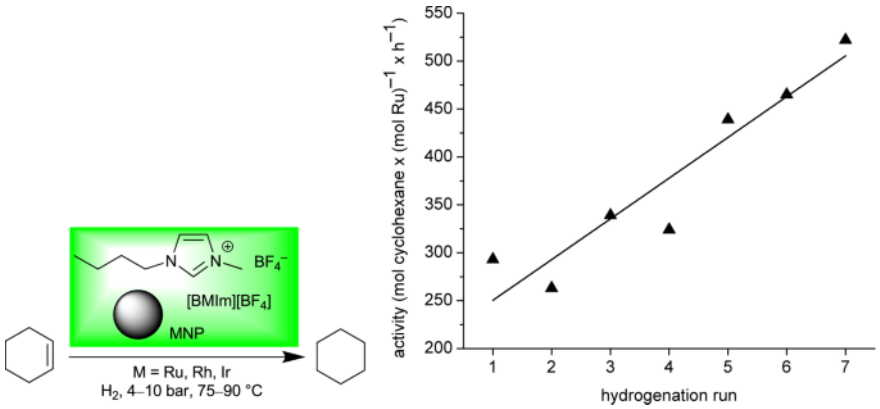

Fig. 18 (color online). Activity for seven runs of the hydrogenation of cyclohexene with the same Ru-NP/[BMIm][BF_4] catalyst at 90 °C, 10 bar H_2 pressure, conversion to 95 % [85].

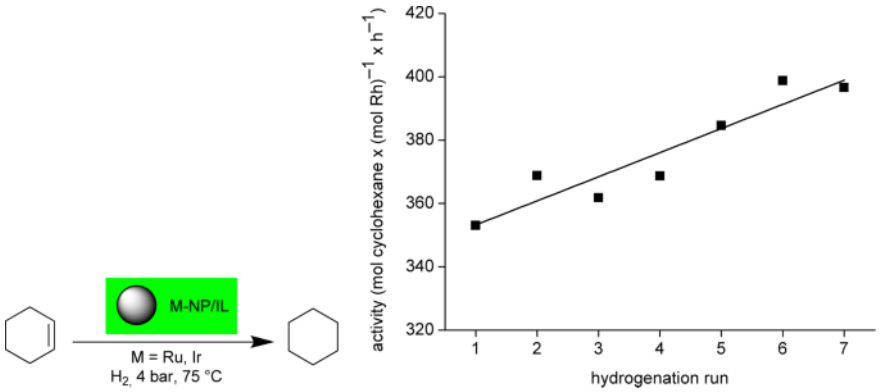

Fig. 19 (color online). Activity over seven catalytic runs for the hydrogenation of cyclohexene with the same Rh-NP/[BMIm][BF_4] catalyst at 75 °C, 4 bar H_2 pressure and 2.5 h reaction time. An activity of 350 mol product per mol Rh per h corresponds to 88 % and an activity of 400 to quantitative (100 %) conversion. With the homologous Ir-NP/[BMIm][BF_4] catalyst even higher activities up to 1900 mol cyclohexane per mol Ir per h could be obtained under similar conditions, but with less metal and with a shorter reaction time of 1 h for near quantitative conversion [96]. (Reprinted from ref. [30] with permission from the author; © 2011 Elsevier B. V.).

The hydrogenation of internal alkynes with Pd-NPs at 25 °C and under 1 bar of hydrogen yields *Z*-alkenes with up to 98 % selectivity. At higher hydrogen pressure (4 bar) alkanes were obtained exlusively without the detection of any alkenes. TOF values were up to 1282 h^{-1} with a good recyclability of the system and no loss of activity for at least 4 runs [112].

Ru-, Rh- and Ir-NP/[BMIm][BF_4] dispersions were active catalysts in the biphasic liquid-liquid hydrogenation of cyclohexene or benzene to cyclohexane [30, 85, 96]. Even a remarkable partial hydrogenation of benzene to cyclohexene could be achieved with Ru-NP/[BMIm][PF_6] dispersions [214]. The low miscibility of substrates and products with the IL phase allows for easy separation by simple decantation of the hydrophobic phase [220]. The hydrogenation reaction of cyclohexene was run at 90 °C and 10 bar H_2 to 95 % conversion where the reaction was intentionally stopped as thereafter the decrease in cyclohexene concentration lowered the reaction rate (Fig. 18) [85].

Rh- and Ir-NP/IL systems function as highly effective and recyclable catalysts in the biphasic liquid-liquid hydrogenation of cyclohexene to cyclohexane with activities of up to 1900 mol cyclohexane per mol Ir per h and 380 mol cyclohexane per mol Rh per h for quantitative conversion at 4 bar H_2 pressure and 75 °C (Fig. 19) [96].

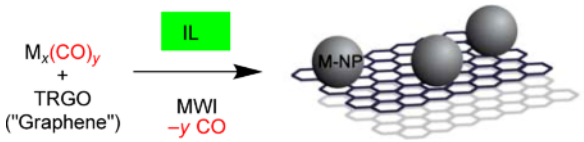

Fig. 20 (color online). The use of microwave irradiation for the synthesis of transition metal nanoparticles supported on thermally reduced graphene oxide (TRGO, schematic presentation) in ILs [224].

Fe-, Ru- and bimetallic Fe-Ru-NPs were tested as catalysts in [BMIm][BF_4] and [BMIm][PF_6] for the hydrogenation of cyclohexenone to mostly cyclohexanone and partly cyclohexanol at 50 °C. The bimetallic FeRu (1 : 1) alloy NPs were most active, followed by the pure Ru-NPs. Addition of CO_2 to the IL reaction mixture increased the reaction rate up to four times faster with 60 bar of CO_2 than without. At 60 bar of CO_2 a high selectivity > 95 % to cyclohexanone, at a TOF of *ca.* 300 h^{-1}, was achieved and the catalyst could be reused 5 times without noticeable deactivation [208].

Stable ruthenium or rhodium metal nanoparticles could be supported on thermally reduced graphene oxide (TRGO) (chemically derived graphene, CDG) surfaces with small and uniform particle sizes (Ru 2.2 ± 0.4 nm and Rh 2.8 ± 0.5 nm) by decomposition of their metal carbonyl precursors $Ru_3(CO)_{12}$ and $Rh_6(CO)_{16}$, respectively, through microwave irradiation in a suspension of TRGO in [BMIm][BF_4] (Figs. 20 and 21). The obtained hybrid nanomaterials Rh-NP/TRGO and Ru-NP/TRGO were – without further treatment – catalytically active in hydrogenation reactions yielding complete conversion of cyclohexene or benzene to cyclohexane under organic-solvent-free

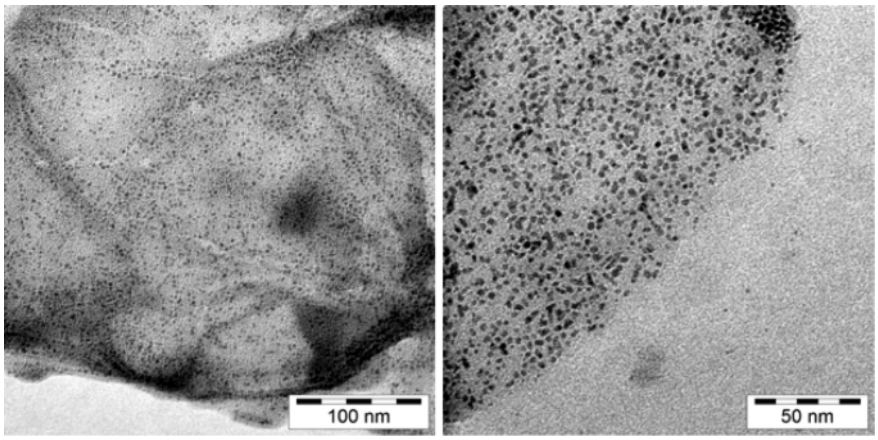

Fig. 21. TEM photographs. Left: Ru-NP supported on thermally reduced graphene oxide (TRGO). Right: Rh-NP on TRGO, from microwave irradiation of $Ru_3(CO)_{12}$ and $Rh_6(CO)_{16}$, respectively, in a TRGO/[BMIm][BF_4] dispersion [224]. (Reprinted from ref. [224] with permission from the author; © 2010 Elsevier Ltd.).

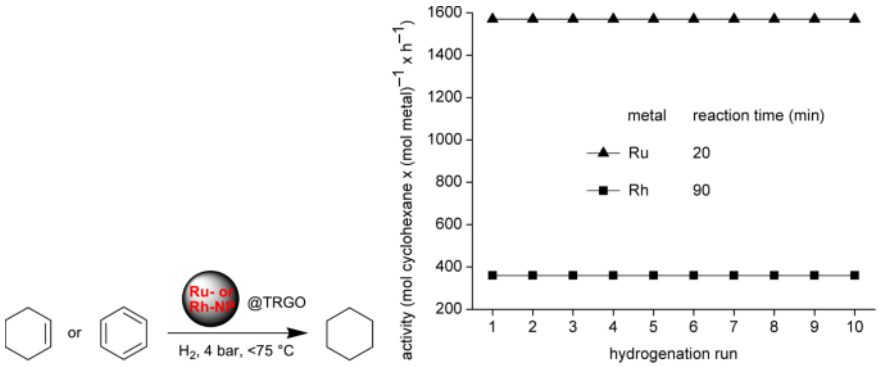

Fig. 22. Activities for the hydrogenation of cyclohexene to cyclohexane with the same M-NP/TRGO catalyst in 10 consecutive runs [224]. (Adapted from ref. [224] with permission from the author; © 2010 Elsevier Ltd.).

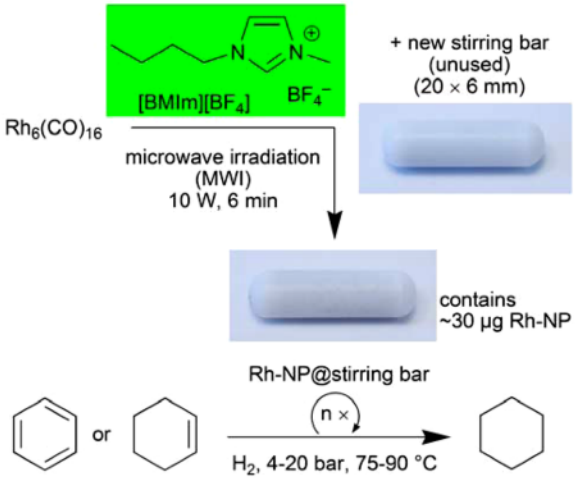

Fig. 23 (color online). Rh-NP deposition on a Teflon-coated magnetic stirring bar from an IL dispersion and the use of a Rh-NP@stirring bar in hydrogenation catalysis [212].

and mild conditions (50 – 75 °C, 4 bar H_2) with reproducible turnovers of 1570 mol cyclohexene per mol Ru per h and 310 mol benzene per mol Rh per h. The catalytically active M-NP/TRGO nanocomposite material could be recycled and used for several runs without any loss of activity (Fig. 22) [224].

Rhodium nanoparticles were reproducibly deposited onto a standard, commercial Teflon-coated magnetic stirring bar by easy and rapid microwave-assisted decomposition of the metal carbonyl precursor $Rh_6(CO)_{16}$ in [BMIm][BF_4]. Such metal nanoparticle deposits are not easy to remove from the Teflon surface by simple washing procedures and present active catalysts which one is not necessarily aware of. Such barely visible metal-nanoparticle deposits on a stirring bar can act as trace metal impurities in catalytic reactions. The rhodium-nanoparticle deposits of 32 μg or less Rh metal on a 20 × 6 mm magnetic stirring bar were shown to catalyze the hydrogenation reaction of neat cyclohexene or benzene to cyclohexane with quantitative conversion. Rhodium nanoparticle-coated stirring bars are easily handled, separable and re-usable catalysts for the heterogeneous hydrogenation with quantitative conversion and very high turnover frequencies of up to 32 800 mol cyclohexene per mol Rh per h under organic-solvent-free conditions (Fig. 23) [212].

Conclusion

In this review it has been shown that ionic liquids are remarkable and excellent media for the synthesis and stabilization of metal nanoparticles (M-NPs) without the need of additional stabilizers, surfactants or capping ligands. ILs can be regarded as supramolecular three-dimensional electrostatic and hydrogen-bonded networks. The stabilization of metal nanoparticles in ILs can be further attributed to effects from the network properties of ILs such as hydrogen bonding, the hydrophobicity and steric interactions which prevent M-NPs agglomeration. Various methods of chemical synthesis for metal nanoparticles in ILs allow for the design of a variety of M-NP shapes and sizes. The synthesis of M-NPs can proceed by chemical reduction, thermolysis, photochemical decomposition, electroreduction, microwave and sonochemical irradiation, as well as gas-phase deposition methods. A microwave-induced thermal decomposition of metal carbonyls $M_x(CO)_y$ in ILs provides an especially rapid and energy-saving access to M-NPs because of the ILs significant absorption efficiency for microwave energy due to their high ionic charge, high polarity and high dielectric constant. Metal carbonyls present attractive synthons as they are readily commercially available and contain the metal atoms already in the zero-valent oxidation state needed for M-NPs. No extra reducing agent is necessary and the only side product CO is given off to the gas phase and removed from the dispersion, thereby largely avoiding contaminations of the M-NP/IL dispersion.

Acknowledgement

The Deutsche Forschungsgemeinschaft is thanked for support through grant Ja466/17-1.

[1] S.-H. Yu, L. R. MacGillivray, C. Janiak, *CrystEngComm* **2012**, *14*, 7531 – 7534.
[2] Z. Peng, H. Yang, *Nano Today* **2009**, *4*, 143 – 164.
[3] A. H. Lu, E. L. Salabas, F. Schüth, *Angew. Chem. Int. Ed.* **2007**, *46*, 1222 – 1244.
[4] A. Gedanken, *Ultrason. Sonochem.* **2004**, *11*, 47 – 55.
[5] C. N. R. Rao, S. R. C. Vivekchand, K. Biswas, A. Govindaraj, *Dalton Trans.* **2007**, 3728 – 3749.

[6] Y. Mastai, A. Gedanken in *Chemistry of Nanomaterials*, Vol. 1 (Eds.: C. N. R. Rao, A. Müller, A. K. Cheetham), Wiley-VCH, Weinheim, **2004**, p. 113.
[7] J. Park, J. Joo, S. G. Kwon, Y. Jang, T. Hyeon, *Angew. Chem. Int. Ed.* **2007**, *46*, 4630 – 4660.
[8] K. An, S. Alayoglu, T. Ewers, G. A. Somorjai, *J. Colloid Interface Sci.* **2012**, *373*, 1 – 13.
[9] M. Kim, V. N. Phan, K. Lee, *CrystEngComm* **2012**, *14*, 7535 – 7548.
[10] J. D. Scholten, B. C. Leal, J. Dupont, *ACS Catal.* **2012**, *2*, 184 – 200.
[11] N. Yan, C. Xiao, Y. Kou, *Coord. Chem. Rev.* **2010**, *254*, 1179 – 1218.
[12] V. I. Pârvulescu, C. Hardacre, *Chem. Rev.* **2007**, *107*, 2615 – 2665.
[13] A. Welther, A. Jacobi von Wangelin, *Curr. Org. Chem.* **2013**, *17*, 326 – 335.
[14] P. S. Campbell, M. H. G. Prechtl, C. C. Santini, P. H. Haumesser, *Curr. Org. Chem.* **2013**, *17*, 414 – 429.
[15] M. Guerrero, N. T. Than Chau, S. Noël, A. Denicourt-Nowicki, F. Hapiot, A. Roucoux, E. Monflier, K. Philippot, *Curr. Org. Chem.* **2013**, *17*, 364 – 399.
[16] J. D. Scholten, *Curr. Org. Chem.* **2013**, *17*, 348 – 363.
[17] W. Ostwald, *Z. Phys. Chem.* **1901**, *37*, 385.
[18] W. Ostwald, *Lehrbuch der Allgemeinen Chemie*, Vol. 2, Part 1, Leipzig, **1896**.
[19] H. Bönnemann, R. M. Richards, *Eur. J. Inorg. Chem.* **2001**, 2455 – 2480.
[20] D. Astruc, F. Lu, J. R. Aranzaes, *Angew. Chem. Int. Ed.* **2005**, *44*, 7852 – 7872.
[21] C. Pan, K. Pelzer, K. Philippot, B. Chaudret, F. Dassenoy, P. Lecante, M.-J. Casanove, *J. Am. Chem. Soc.* **2001**, *123*, 7584 – 7593.
[22] J. D. Aiken III, R. G. Finke, *J. Am. Chem. Soc.* **1999**, *121*, 8803 – 8810.
[23] J. Krämer, E. Redel, R. Thomann, C. Janiak, *Organometallics* **2008**, *27*, 1976 – 1978.
[24] K. Ueno, H. Tokuda, M. Watanabe, *Phys. Chem. Chem. Phys.* **2010**, *12*, 1649 – 1658.
[25] J. Dupont, J. D. Scholten, *Chem. Soc. Rev.* **2010**, *39*, 1780 – 1804.
[26] J. Dupont, *J. Braz. Chem. Soc.* **2004**, *15*, 341 – 350.
[27] M.-A. Neouze, *J. Mater. Chem.* **2010**, *20*, 9593 – 9607.
[28] C. S. Consorti, P. A. Z. Suarez, R. F. de Souza, R. A. Burrow, D. H. Farrar, A. J. Lough, W. Loh, L. H. M. da Silva, J. Dupont, *J. Phys. Chem. B* **2005**, *109*, 4341 – 4349.
[29] J. Dupont, P. A. Z. Suarez, R. F. de Souza, R. A. Burrow, J.-P. Kintzinger, *Chem. Eur. J.* **2000**, *6*, 2377 – 2381.
[30] C. Vollmer, C. Janiak, *Coord. Chem. Rev.* **2011**, *255*, 2039 – 2057.
[31] H. Weingärtner, *Angew. Chem. Int. Ed.* **2008**, *47*, 654 – 670.
[32] D. Xiao, J. R. Rajian, A. Cady, S. Li, R. A. Bartsch, E. L. Quitevis, *J. Phys. Chem. B* **2007**, *111*, 4669 – 4677.
[33] S. Kuwabata, T. Tsuda, T. Torimoto, *J. Phys. Chem. Lett.* **2010**, *1*, 3177 – 3188.
[34] P. Wasserscheid, W. Keim, *Angew. Chem. Int. Ed.* **2000**, *39*, 3772 – 3789.
[35] I. Krossing, J. M. Slattery, C. Daguenet, P. J. Dyson, A. Oleinikova, H. Weingärtner, *J. Am. Chem. Soc.* **2006**, *128*, 13427 – 13434.
[36] K. R. Seddon, *Chem. Soc. Rev.* **2008**, *37*, 123 – 150.
[37] T. Welton, *Chem. Rev.* **1999**, *99*, 2071 – 2084.
[38] J. P. Hallett, T. Welton, *Chem. Rev.* **2011**, *111*, 3508 – 3576.
[39] T. Torimoto, T. Tsuda, K. Okazaki, S. Kuwabata, *Adv. Mater.* **2010**, *22*, 1196 – 1221.
[40] R. E. Morris, *Chem. Commun.* **2009**, 2990 – 2998.
[41] E. R. Parnham, R. E. Morris, *Acc. Chem. Res.* **2007**, *40*, 1005 – 1013.
[42] E. R. Cooper, C. D. Andrews, P. S. Wheatley, P. B. Webb, P. Wormald, R. E. Morris, *Nature* **2004**, *430*, 1012 – 1016.
[43] Y. Lin, S. Dehnen, *Inorg. Chem.* **2011**, *50*, 7913 – 7915.
[44] T. P. Lodge, *Science* **2008**, *321*, 50 – 51.
[45] P. Bonhôte, A.-P. Dias, N. Papageorgiou, K. K. Kalyanasundaram, M. Grätzel, *Inorg. Chem.* **1996**, *35*, 1168 – 1178.
[46] J. M. Pringle, J. Golding, K. Baranyai, C. M. Forsyth, G. B. Deacon, J. L. Scott, D. R. MacFarlane, *New J. Chem.* **2003**, *27*, 1504 – 1510.
[47] T. J. Gannon, G. Law, R. P. Watson, A. J. Carmichael, K. R. Seddon, *Langmuir* **1999**, *15*, 8429 – 8434.
[48] J. N. A Canongia Lopes, M. F. C. Gomes, A. A. H. Padua, *J. Phys. Chem. B* **2006**, *110*, 16816 – 16818.
[49] G. Law, R. P. Watson, A. J. Carmichael, K. R. Seddon, *Phys. Chem. Chem. Phys.* **2001**, *3*, 2879 – 2885.
[50] J. N. A. Canongia Lopes, A. A. H. Pádua, *J. Phys. Chem. B* **2006**, *110*, 3330 – 3335.
[51] C. N. R. Rao, H. S. S. R. Matte, R. Voggu, A. Govindaraj, *Dalton Trans.* **2012**, *41*, 5089 – 5120.
[52] H. Zhang, H. Cui, *Langmuir* **2009**, *25*, 2604 – 2612.
[53] H. S. Schrekker, M. A. Gelesky, M. P. Stracke, C. M. L. Schrekker, G. Machado, S. R. Teixeira, J. C. Rubim, J. Dupont, *J. Colloid Interface Sci.* **2007**, *316*, 189 – 195.
[54] R. A. Alvarez-Puebla, E. Arceo, P. J. G. Goulet, J. J. Garrido, R. F. Aroca, *J. Phys. Chem. B* **2005**, *109*, 3787 – 3792.

[55] E. J. W. Verwey, J. T. G. Overbeek, *Theory of the Stability of Lyophobic Colloids*, Dover Publications, Mineola, New York, **1999**, pp. 1 – 218.
[56] E. Redel, J. Krämer, R. Thomann, C. Janiak, *GIT Labor-Fachzeitschrift*, **2008**, April, 400 – 404.
[57] A. N. Shipway, E. Katz, I. Willner, *ChemPhysChem* **2000**, *1*, 18 – 25.
[58] T. Cassagneau, J. H. Fendler, *J. Phys. Chem. B* **1999**, *103*, 1789 – 1793.
[59] C. D. Keating, K. K. Kovaleski, M. J. Natan, *J. Phys. Chem. B* **1998**, *102*, 9404 – 9413.
[60] M. N. Kobrak, H. Li, *Phys. Chem. Chem. Phys.* **2010**, *12*, 1922 – 1932.
[61] G. Schmid in *Nanoparticles: From Theory to Applications*, (Ed.: G. Schmid), 2nd ed., Wiley-VCH, Weinheim, **2010**, pp. 214 – 238.
[62] L. S. Ott, R. G. Finke, *Coord. Chem. Rev.* **2007**, *251*, 1075 – 1100.
[63] B. L. Bhargava, S. Balasubramanian, M. L. Klein, *Chem. Commun.* **2008**, 3339 – 3351.
[64] E. Redel, M. Walter, R. Thomann, C. Vollmer, L. Hussein, H. Scherer, M. Krüger, C. Janiak, *Chem. Eur. J.* **2009**, *15*, 10047 – 10059.
[65] E. Redel, M. Walter, R. Thomann, L. Hussein, M. Krüger, C. Janiak, *Chem. Commun.* **2010**, *46*, 1159 – 1161.
[66] S. A. Katsyuba, E. E. Zvereva, N. Yan, X. Yuan, Y. Kou, P. J. Dyson, *ChemPhysChem* **2012**, *13*, 1781 – 1790.
[67] H. Itoh, K. Naka, Y. Chujo, *J. Am. Chem. Soc.* **2004**, *126*, 3026 – 3027.
[68] K.-S. Kim, D. Demberelnyamba, H. Lee, *Langmuir* **2004**, *20*, 556 – 560.
[69] S. Gao, H. Zhang, X. Wang, W. Mai, C. Peng, L. Ge, *Nanotechnology* **2005**, *16*, 1234 – 1237.
[70] R. Marcilla, D. Mecerreyes, I. Odriozola, J. A. Pomposo, J. Rodriguez, I. Zalakain, I. Mondragon, *Nano* **2007**, *2*, 169 – 173.
[71] L. C. Branco, N. J. Rosa, J. J. M. Ramos, C. A. M. Alfonso, *Chem. Eur. J.* **2002**, *8*, 3671 – 3677.
[72] X. Yuan, N. Yan, S. A. Katsyuba, E. Zvereva, Y. Kou, P. J. Dyson, *Phys. Chem. Chem. Phys.* **2012**, *14*, 6026 – 6033.
[73] D. Zhao, Z. Fei, R. Scopelliti, P. Dyson, *Inorg. Chem.* **2004**, *43*, 2197 – 2205.
[74] D. Zhao, Z. Fei, T. J. Geldbach, R. Scopeliti, P. Dyson, *J. Am. Chem. Soc.* **2004**, *126*, 15876 – 15882.
[75] M. H. G. Prechtl, J. D. Scholten, J. Dupont, *J. Mol. Catal. A* **2009**, *313*, 74 – 78.
[76] A. Taubert, *Top. Curr. Chem.* **2010**, *290*, 127 – 159.
[77] D.-P. Liu, G.-D. Li, Y. Su, J.-S. Chen, *Angew. Chem. Int. Ed.* **2006**, *45*, 7370 – 7373.
[78] D. Marquardt, Z. Xie, A. Taubert, R. Thomann, C. Janiak, *Dalton Trans.* **2011**, *40*, 8290 – 8293.
[79] A. Taubert, Z. Li, *Dalton Trans.* **2007**, 723 – 727.
[80] E. Redel, R. Thomann, C. Janiak, *Inorg. Chem.* **2008**, *47*, 14 – 16.
[81] L. S. Ott, R. G. Finke, *Inorg. Chem.* **2006**, *45*, 8382 – 8393.
[82] G. S. Fonseca, A. P. Umpierre, P. F. P. Fichtner, S. R. Teixeira, J. Dupont, *Chem. Eur. J.* **2003**, *9*, 3263 – 3269.
[83] Z. Li, A. Friedrich, A. Taubert, *J. Mater. Chem.* **2008**, *18*, 1008 – 1014.
[84] P. Migowski, D. Zanchet, G. Machado, M. A. Gelesky, S. R. Teixeira, J. Dupont, *Phys. Chem. Chem. Phys.* **2010**, *12*, 6826 – 6833.
[85] C. Vollmer, E. Redel, K. Abu-Shandi, R. Thomann, H. Manyar, C. Hardacre, C. Janiak, *Chem. Eur. J.* **2010**, *16*, 3849 – 3858.
[86] P. Migowski, G. Machado, S. R. Teixeira, M. C. M. Alves, J. Morais, A. Traverse, J. Dupont, *Phys. Chem. Chem. Phys.* **2007**, *9*, 4814 – 4821.
[87] M. Ruta, G. Laurenczy, P. J. Dyson, L. Kiwi-Minsker, *J. Phys. Chem. C* **2008**, *112*, 17814 – 17819.
[88] R. R. Deshmukh, R. Rajagopal, K. V. Srinivasan, *Chem. Commun.* **2001**, 1544 – 1545.
[89] K. Anderson, S. C. Fernández, C. Hardacre, P. C. Marr, *Inorg. Chem. Commun.* **2004**, *7*, 73 – 76.
[90] J. M. Zhu, Y. H. Shen, A. J. Xie, L. G. Qiu, Q. Zhang, X. Y. Zhang, *J. Phys. Chem. C* **2007**, *111*, 7629 – 7633.
[91] M. A. Firestone, M. L. Dietz, S. Seifert, S. Trasobares, D. J. Miller, N. J. Zaluzec, *Small* **2005**, *1*, 754 – 760.
[92] K. Peppler, M. Polleth, S. Meiss, M. Rohnke, J. Janek, *Z. Phys. Chem.* **2006**, *220*, 1507 – 1527.
[93] A. Safavi, N. Maleki, F. Tajabadi, E. Farjami, *Electrochem. Commun.* **2007**, *9*, 1963 – 1968.
[94] K. Kim, C. Lang, P. A. Kohl, *J. Electrochem. Soc.* **2005**, *152*, E9 – E13.
[95] E. Redel, R. Thomann, C. Janiak, *Chem. Commun.* **2008**, 1789 – 1791.
[96] E. Redel, J. Krämer, R. Thomann, C. Janiak, *J. Organomet. Chem.* **2009**, *694*, 1069 – 1075.
[97] T. Gutel, J. Garcia-Anton, K. Pelzer, K. Philippot, C. C. Santini, Y. Chauvin, B. Chaudret, J.-M. Basset, *J. Mater. Chem.* **2007**, *17*, 3290 – 3292.
[98] G. Salas, A. Podgorsek, P. S. Campbell, C. C. Santini, A. A. H. Pádua, M. F. Costa Gomes, K. Philippot, B. Chaudret, M. Turmine, *Phys. Chem. Chem. Phys.* **2011**, *13*, 13527 – 13536.
[99] M. Antonietti, D. Kuang, B. Smarly, Y. Zhou, *Angew. Chem. Int. Ed.* **2004**, *43*, 4988 – 4922.
[100] K. I. Hana, S. W. Kang, J. Kima, Y. S. Kang, *J. Membr. Sci.* **2011**, *374*, 43 – 48.

[101] J. Dupont, G. S. Fonseca, A. P. Umpierre, P. F. P. Fichtner, S. R. Teixeira, *J. Am. Chem. Soc.* **2002**, *124*, 4228 – 4229.

[102] C. W. Scheeren, G. Machado, J. Dupont, P. F. P. Fichtner, S. R. Texeira, *Inorg. Chem.* **2003**, *42*, 4738 – 4742.

[103] A. I. Bhatt, A. Mechler, L. L. Martin, A. M. Bond, *J. Mater. Chem.* **2007**, *17*, 2241 – 2250.

[104] M. A. Gelesky, A. P. Umpierre, G. Machado, R. R. B. Correia, W. C. Magno, J. Morais, G. Ebeling, J. Dupont, *J. Am. Chem. Soc.* **2007**, *127*, 4588 – 4589.

[105] R. R. Dykeman, N. Yan, R. Scopelliti, P. J. Dyson, *Inorg. Chem.* **2011**, *50*, 717 – 719.

[106] G. S. Fonseca, G. Machado, S. R. Teixeira, G. H. Fecher, J. Morais, M. C. M. Alves, J. Dupont, *J. Colloid Interface Sci.* **2006**, *301*, 193 – 204.

[107] X. Zhao, Y. Hua, L. Liang, C. Liu, J. Liao, W. Xing, *Int. J. Hydrogen Energy* **2012**, *37*, 51 – 58.

[108] X. Yuan, G. Sun, H. Asakura, T. Tanaka, X. Chen, Y. Yuan, G. Laurenczy, Y. Kou, P. J. Dyson, N. Yan, *Chem. Eur. J.* **2013**, *19*, 1227 – 1234.

[109] V. Caló, A. Nacci, A. Monopoli, S. Laera, N. Cioffi, *J. Org. Chem.* **2003**, *68*, 2929 – 2933.

[110] V. Caló, A. Nacci, A. Monopoli, A. Detomaso, P. Iliade, *Organometallics* **2003**, *22*, 4193 – 4197.

[111] F. Hassine, M. Pucheault, M. Vaultier, *C. R. Chimie* **2011**, *14*, 671 – 679.

[112] R. Venkatesan, M. H. G. Prechtl, J. D. Scholten, R. P. Pezzi, G. Machado, J. Dupont, *J. Mater. Chem.* **2011**, *21*, 3030 – 3036.

[113] M. Planellas, R. Pleixats, A. Shafir, *Adv. Synth. Catal.* **2012**, *354*, 651 – 662.

[114] M. J. Beier, J.-M. Andanson, A. Baiker, *ACS Catalysis* **2012**, *2*, 2587 – 2595.

[115] M. J. Baier, J.-M. Andanson, T. Mallat, F. Krumeich, A. Baiker, *ACS Catalysis* **2012**, *2*, 337 – 340.

[116] C. W. Scheeren, J. B. Domingos, G. Machado, J. Dupont, *J. Phys. Chem. C* **2008**, *112*, 16463 – 16469.

[117] D. Marquardt, J. Barthel, M. Braun, C. Ganter, C. Janiak, *CrystEngComm* **2012**, *14*, 7607 – 7615.

[118] D. Raut, K. Wankhede, V. Vaidya, S. Bhilare, N. Darwatkar, A. Deorukhkar, G. Trivedi, M. Salunkhe, *Catal. Commun.* **2009**, *10*, 1240 – 1243.

[119] P. Setua, R. Pramanik, S. Sarkar, C. Ghatak, V. G. Rao, N. Sarkar, S. K. Das, *J. Mol. Liq.* **2011**, *162*, 33 – 37.

[120] L. L. Larazus, C. T. Riche, N. Malmstadt, R. L. Brutchey, *Langmuir* **2012**, *28*, 15987 – 15993.

[121] T. Dai, L. Ge, R. Guo, *J. Mater. Res.* **2009**, *24*, 333 – 341.

[122] J. M. Obliosca, I. Harvey, J. Arellano, M. H. Huang, S. D. Arco, *Mater. Lett.* **2010**, *64*, 1109 – 1112.

[123] X. Bai, X. Li, L. Zheng, *Langmuir* **2010**, *26*, 12209 – 12214.

[124] L. Casal-Dujat, M. Rodrigues, A. Yagüe, A. C. Calpena, D. B. Amabilino, J. González-Linares, M. Borras, L. Pérez-García, *Langmuir* **2012**, *28*, 2368 – 2381.

[125] L. L. Lazarus, A. S.-J. Yang, S. Chu, R. L. Brutchey, N. Malmstadt, *Lab Chip* **2010**, *10*, 3377 – 3379.

[126] P. Dash, S. M. Miller, R. W. J. Scott, *J. Mol. Catal. A: Chem.* **2010**, *329*, 86 – 95.

[127] A. Safavi, S. Zeinali, *Colloids Surf. A: Physicochem. Eng. Asp.* **2010**, *362*, 121 – 126.

[128] Z. Li, A. Taubert, *Molecules* **2009**, *14*, 4682 – 4688.

[129] V. Khare, Z. Li, A. Mantion, A. A. Ayi, S. Sonkaria, A. Voelkl, A. F. Thünemann, A. Taubert, *J. Mater. Chem.* **2010**, *20*, 1332 – 1339.

[130] W. Huang, S. Chen, Y. Liu, H. Fu, G. Wu, *Nanotechnology* **2011**, *22*, 025602.

[131] E. Dinda, M. H. Rashid, M. Biswas, T. K. Mandal, *Langmuir* **2010**, *26*, 17568 – 17580.

[132] G. Zhang, H. Zhou, C. An, D. Liu, Z. Huang, Y. Kuang, *Colloid Polym. Sci.* **2012**, *290*, 1435 – 1441.

[133] L. L. Lazarus, C. T. Riche, B. C. Marin, M. Gupta, N. Malmstadt, R. L. Brutchey, *ACS Appl. Mater. Interfaces* **2012**, *4*, 3077 – 3083.

[134] M. H. G. Prechtl, J. D. Scholten, J. Dupont, *Molecules* **2010**, *15*, 3441 – 3461.

[135] J. D. Scholten, G. Ebeling, J. Dupont, *Dalton Trans.* **2007**, 5554 – 5560.

[136] L. Zhao, C. Zhang, L. Zhuo, Y. Zhang, J. Y. Ying, *J. Am. Chem. Soc.* **2008**, *130*, 12586 – 12587.

[137] T. Tano, K. Esumi, K. Meguro, *J. Colloid Interface Sci.* **1989**, *133*, 530 – 533.

[138] K. Esumi, M. Suzuki, T. Tano, K. Torigoe, K. Meguro, *Colloids Surf.* **1991**, *55*, 9 – 14.

[139] J. S. Bradley, E. W. Hill, C. Klein, B. Chaudret, A. Duteil, *Chem. Mater.* **1993**, *5*, 254 – 256.

[140] U. Schröder, J. D. Wadhawan, R. G. Compton, F. Marken, P. A. Z. Suarez, C. S. Consorti, R. F. de Souza, J. Dupont, *New J. Chem.* **2000**, *24*, 1009 – 1015.

[141] S. Guo, E. Wang, *Anal. Chim. Acta* **2007**, *598*, 181 – 192.

[142] J. Turkevich, P. C. Stevenson, J. Hillier, *Discuss. Faraday Soc.* **1951**, *11*, 55 – 75.

[143] H. R. Ryu, L. Sanchez, H. A. Keul, A. Raj, M. R. Bockstaller, *Angew. Chem. Int. Ed.* **2008**, *47*, 7639 – 7643.

[144] T. A. Ryan, C. Ryan, E. A. Seddon, K. R. Seddon in *Phosgene and Related Carbonyl Halides*, Monograph 24 in *Topics in Inorganic and General Chemistry* (Ed.: R. J. H. Clark), Elsevier, Amsterdam, **1996**, p. 242.

[145] S. F. L. Mertens, C. Vollmer, A. Held, M. H. Aguirre, M. Walter, C. Janiak, T. Wandlowski, *Angew. Chem. Int. Ed.* **2011**, *50*, 9735 – 9738.

[146] H. Hosseini-Monfared, H. Meyer, C. Janiak, *J. Mol. Catal. A: Chem.* **2013**, *372*, 72 – 78.

[147] A. Corma, I. Domínguez, T. Ródenas, M. J. Sabater, *J. Catal.* **2008**, *259*, 26 – 35.

[148] S. Miao, Z. Liu, Z. Zhang, B. Han, Z. Miao, K. Ding, G. An, *J. Phys. Chem. C* **2007**, *111*, 2185 – 2190.

[149] D. Marquardt, F. Beckert, F. Pennetreau, F. Tölle, R. Mülhaupt, O. Riant, S. Hermans, J. Barthel, C. Janiak, *Carbon* **2013**, in press; DOI: 10.1016/j.carbon.2013.09.002.

[150] D. Marquardt, C. Janiak, *Nachr. Chemie* **2013**, *61*, 754 – 757.

[151] P. Dash, R. W. J. Scott, *Mater. Lett.* **2011**, *65*, 7 – 9.

[152] M. Harada, Y. Kimura, K. Saijo, T. Ogawa, S. Isoda, *J. Colloid Interface Sci.* **2009**, *339*, 373 – 381.

[153] H. Park, J.-S. Kim, B. G. Choi, S. M. Jo, D. Y. Kim, W. H. Hong, S.-Y. Jang, *Carbon* **2010**, *48*, 1325 – 1330.

[154] Z. Wang, Q. Zhang, D. Kuehner, X. Xu, A. Ivaska, L. Niu, *Carbon* **2008**, *46*, 1687 – 1692.

[155] F. Endres, *ChemPhysChem* **2002**, *3*, 144 – 154.

[156] F. Endres, D. MacFarlane, A. Abbott, *Electrodeposition from Ionic Liquids*, Wiley-VCH Verlag, Weinheim, **2008**.

[157] U. Erb, US patent, US 5352266, **1994**.

[158] H. Natter, T. Krajewski, R. Hempelmann, *Ber. Bunsenges. Phys. Chem.* **1996**, *100*, 55 – 64.

[159] H. Natter, R. Hempelmann, *J. Phys. Chem.* **1996**, *100*, 19525 – 19532.

[160] H. Natter, M. Schmelzer, M.-S. Löffler, C. E. Krill, A. Fitch, R. Hempelmann, *J. Phys. Chem. B* **2000**, *104*, 2467 – 2476.

[161] R. Przenioslo, J. Wagner, H. Natter, R. Hempelmann, W. Wagner, *J. Alloys Compd.* **2001**, *328*, 259 – 263.

[162] H. Natter, M. Schmelzer, R. Hempelmann, *J. Mater. Res.* **1998**, *13*, 1186 – 1197.

[163] H. Natter, M. Bukowski, R. Hempelmann, S. Zein El Abedin, E. M. Moustafa, F. Endres, *Z. Phys. Chem. B* **2006**, *220*, 1275 – 1291.

[164] L. Yu, H. Sun, J. He, D. Wang, X. Jin, X. Hu, G. Z. Chen, *Electrochem. Commun.* **2007**, *9*, 1374 – 1381.

[165] P. Roy, R. Lynch, P. Schmuki, *Electrochem. Commun.* **2009**, *11*, 1567 – 1570.

[166] S. Zein El Abedin, F. Endres, *Electrochim. Acta* **2009**, *54*, 5673 – 5677.

[167] D. Wei, J. K. Baral, R. Österbacka, A. Ivaska, *J. Mater. Chem.* **2008**, *18*, 1853 – 1857.

[168] C. Fu, Y. Kuang, Z. Huang, X. Wang, N. Du, J. Chen, H. Zhou, *Chem. Phys. Lett.* **2010**, *499*, 250 – 253.

[169] J.-H. Cha, K.-S. Kim, S. Choi, S.-H. Yeon, H. Lee, C.-S. Lee, J.-J. Shim, *Korean J. Chem. Eng.* **2007**, *24*, 1089 – 1094.

[170] T. A. Kareem, A. A. Kaliani, *Ionics* **2012**, *18*, 315 – 327.

[171] T. Suzuki, K.-I. Okazaki, S. Suzuki, T. Shibayama, S. Kuwabata, T. Torimoto, *Chem. Mater.* **2010**, *22*, 5209 – 5215.

[172] T. Tsuda, K. Yoshii, T. Torimoto, S. Kuwabata, *J. Power Sources* **2010**, *195*, 5980 – 5985.

[173] K. Yoshii, T. Tsuda, T. Arimura, A. Imanishi, T. Torimoto, S. Kuwabata, *RSC Adv.* **2012**, *2*, 8262 – 8264.

[174] Y. Hatakeyama, S. Takahashi, K. Nishikawa, *J. Phys. Chem. C* **2010**, *114*, 11098 – 11102.

[175] T. Kameyama, Y. Ohno, T. Kurimoto, K.-I. Okazaki, T. Uematsu, S. Kuwabata, T. Torimoto, *Phys. Chem. Chem. Phys.* **2010**, *12*, 1804 – 1811.

[176] H. Wender, L. F. de Oliveira, P. Migowski, A. F. Feil, E. Lissner, M. H. G. Prechtl, S. R. Teixeira, J. Dupont, *J. Phys. Chem. C* **2010**, *114*, 11764 – 11768.

[177] Q. Chen, T. Kaneko, R. Hatakeyama, *Current Applied Physics* **2011**, *11*, S63 – S66.

[178] T. Kaneko, K. Baba, R. Hatakeyama, *J. Appl. Phys.* **2009**, *105*, 103306-1 – 103306-5.

[179] Y.-B. Xie, C.-J. Liu, *Plasma Processes Polym.* **2008**, *5*, 239 – 245.

[180] S. Zein El Abedin, M. Pölleth, S. A. Meiss, J. Janek, F. Endres, *Green Chem.* **2007**, *9*, 549 – 553.

[181] M. Brettholle, O. Höfft, L. Klarhöfer, S. Mathes, W. Maus-Friedrichs, S. Zein El Abedin, S. Krischok, J. Janek, F. Endres, *Phys. Chem. Chem. Phys.* **2010**, *12*, 1750 – 1755.

[182] S. A. Meiss, M. Rohnke, L. Kienle, S. Zein El Abedin, F. Endres, J. Janek, *ChemPhysChem* **2007**, *8*, 50 – 53.

[183] P. He, H. Liu, Z. Li, Y. Liu, X. Xu, J. Li, *Langmuir* **2004**, *20*, 10260 – 10267.

[184] Z. Wei, C.-J. Liu, *Mater. Lett.* **2011**, *65*, 353 – 355.

[185] A. A. Aal, R. Al-Salman, M. Al-Zoubi, N. Borissenko, F. Endres, O. Höfft, A. Prowald, S. Zein El Abedin, *Electrochim. Acta* **2011**, *56*, 10295 – 10305.

[186] K. Richter, A. Birkner, A.-V. Mudring, *Angew. Chem. Int. Ed.* **2010**, *49*, 2431 – 2435.

[187] K. Richter, A. Birkner, A.-V. Mudring, *Phys. Chem. Chem. Phys.* **2011**, *13*, 7136 – 7141.

[188] T. Tsuda, S. Seino, S. Kuwabata, *Chem. Commun.* **2009**, 6792 – 6794.

[189] A. Imanishi, M. Tamura, S. Kuwabata, *Chem. Commun.* **2009**, 1775 – 1777.

[190] D. G. E. Kerfoot, X. Nickel, E. Wildermuth, H. Stark, G. Friedrich, F. L. Ebenhöch, B. Kühborth, J. Silver, R. Rituper in *Ullmann's Encyclopaedia of Industrial*

Chemistry, 5th ed. online, Wiley-VCH, Weinheim, **2008**.
[191] T. Hyeon, *Chem. Commun.* **2003**, 927 – 934.
[192] M. Larhed, C. Moberg, A. Hallberg, *Acc. Chem. Res.* **2002**, *35*, 717 – 727.
[193] D. Bogdal, *Microwave-Assisted Organic Synthesis*, Elsevier, New York, **2006**, pp. 47 – 189.
[194] D. M. P Mingos D. R. Baghurst, *Chem. Soc. Rev.* **1991**, *20*, 1 – 47.
[195] S. A. Galema, *Chem. Soc. Rev.* **1997**, *26*, 233 – 238.
[196] A. L. Buchachenko, E. L. Frankevich, *Chemical Generation and Reception of Radio- and Microwaves*, Wiley-VCH, Weinheim, **1993**, pp. 41 – 56.
[197] V. K. Ahluwulia, *Alternative Energy Processes in Chemical Synthesis*, Alpha Science International LTD, Oxford, **2008**.
[198] I. Bilecka, M. Niederberger, *Nanoscale* **2010**, *2*, 1358 – 1374.
[199] T. S. Ahmadi, S. L. Logunov, M. A. Elsayed, *J. Phys. Chem.* **1996**, *100*, 8053 – 8056.
[200] M. Perner, P. Bost, U. Lemmer, G. von Plessen, J. Feldmann, U. Becker, M. Mennig, M. Schmitt, H. Schmidt, *Phys. Rev. Lett.* **1997**, *78*, 2192 – 2195.
[201] W. Andra, C. D'Ambly, R. Hergt, *J. Magn. Magn. Mater.* **1999**, *194*, 197 – 203.
[202] J. Berlan, P. Giboreau, S. Lefeuvre, C. Marchand, *Tetrahedron Lett.* **1991**, *32*, 2363 – 2366.
[203] F. Langa, P. de la Cruz, A. de la Hoz, A. Diaz-Ortiz, E. Diez-Barra, *Contemp. Org. Synth.* **1997**, *4*, 373 – 386.
[204] L. Perreux, A. Loupy, *Tetrahedron* **2001**, *57*, 9199 – 9233.
[205] A. Stadler, C. O. Kappe, *J. Chem. Soc., Perkin Trans.* **2000**, 1363 – 1368.
[206] A. Stadler, C. O. Kappe, *Eur. J. Org. Chem.* **2001**, 919 – 924.
[207] J. He, Y. Zhang, E. Y.-X. Chen, *ChemSusChem* **2013**, *6*, 61 – 64.
[208] J.-M. Andanson, S. Marx, A. Baiker, *Catal. Sci. Technol.* **2012**, *2*, 1403 – 1409.
[209] D. O. Silva, J. D. Scholten, M. A. Gelesky, S. R. Teixeira, A. C. B. Dos Santos, E. F. Souza-Aguiar, J. Dupont, *ChemSusChem* **2008**, *1*, 291 – 294.
[210] M. Scariot, D. O. Silva, J. D. Scholten, G. Machado, S. R. Teixeira, M. A. Novak, G. Ebeling, J. Dupont, *Angew. Chem. Int. Ed.* **2008**, *47*, 9075 – 9078.
[211] S. Behrens, S. Essig, *J. Mater. Chem.* **2012**, *22*, 3811 – 3816.
[212] C. Vollmer, M. Schröder, Y. Thomann, R. Thomann, C. Janiak, *Appl. Catal. A* **2012**, *425 – 426*, 178 – 183.
[213] G. H. Hong, S. W. Kang, *Ind. Eng. Chem. Res.* **2013**, *52*, 794 – 797.
[214] E. T. Silveira, A. P. Umpierre, L. M. Rossi, G. Machado, J. Morais, G. V. Soares, I. J. R. Baumvol, S. R. Teixeira, R. F. P. Fichtner, J. Dupont, *Chem. Eur. J.* **2004**, *10*, 3734 – 3740.
[215] T. Gutel, C. C. Santini, K. Philippot, A. Padua, K. Pelzer, B. Chaudret, Y. Chauvin, J.-M. Basset, *J. Mater. Chem.* **2009**, *19*, 3624 – 3631.
[216] P. S. Campbell, C. C. Santini, D. Bouchu, B. Fenet, K. Philippot, B. Chaudret, A. A. H. Pádua, Y. Chauvin, *Phys. Chem. Chem. Phys.* **2010**, *12*, 4217 – 4223.
[217] G. Salas, C. C. Santini, K. Philippot, V. Collière, B. Chaudret, B. Fenet, P. F. Fazzini, *Dalton Trans.* **2011**, *40*, 4660 – 4668.
[218] R. A. Sheldon, *Chem. Commun.* **2008**, 3352 – 3365.
[219] P. Wasserscheid, T. Welton in *Ionic Liquids in Synthesis*, Vol. 1, (Eds.: P. Wasserscheid, T. Welton), Wiley-VCH, Weinheim, **2007**, pp. 325 – 350.
[220] C. van Doorslaer, Y. Schellekens, P. Mertens, K. Binnemanns, D. De Vos, *Phys. Chem. Chem. Phys.* **2010**, *12*, 1741 – 1749.
[221] A. D. Sawant, D. G. Raut, N. B. Darvatkar, M. M. Salunkhe, *Green Chem. Lett. Rev.* **2011**, *4*, 41 – 54.
[222] D. Astruc, *Nanoparticles and Catalysis*, Wiley-VCH, New York, **2007**.
[223] J. Dupont, R. F. de Souza, P. A. Z. Suarez, *Chem. Rev.* **2002**, *102*, 3667 – 3692.
[224] D. Marquardt, C. Vollmer, R. Thomann, P. Steurer, R. Mülhaupt, E. Redel, C. Janiak, *Carbon* **2011**, *49*, 1326 – 1332.